

## A Catalogue of H I Selected Galaxies from the South Celestial Cap Region of Sky

V. A. Kilborn,<sup>1,2</sup> R. L. Webster,<sup>1</sup> L. Staveley-Smith,<sup>3</sup> M. Marquarding,<sup>3</sup> G. D. Banks,<sup>4</sup> D. G. Barnes,<sup>5</sup> R. Bhathal,<sup>6</sup> W. J. G. de Blok,<sup>3</sup> P. J. Boyce,<sup>7</sup> M. J. Disney,<sup>4</sup> M. J. Drinkwater,<sup>1</sup> R. D. Ekers,<sup>3</sup> K. C. Freeman,<sup>8</sup> B. K. Gibson,<sup>5</sup> P. A. Henning,<sup>9</sup> M. Howlett,<sup>5</sup> H. Jerjen,<sup>8</sup> P. M. Knezek,<sup>11,17</sup> B. Koribalski,<sup>3</sup> D. F. Malin,<sup>10</sup> R. F. Minchin,<sup>4</sup> J. R. Mould,<sup>8</sup> J. C. O'Brien,<sup>8</sup> T. Oosterloo,<sup>12</sup> P. F. Ortiz,<sup>13</sup> R. M. Price,<sup>3,9</sup> M. E. Putman,<sup>14</sup> S. D. Ryder,<sup>10</sup> E. M. Sadler,<sup>15</sup> I. M. Stewart,<sup>16</sup> F. Stootman,<sup>6</sup> O. I. Wong,<sup>1</sup> and A. E. Wright<sup>3</sup>

### ABSTRACT

The first deep catalogue of the H I Parkes All Sky Survey (HiPASS) is presented, covering the South Celestial Cap (SCC) region. The SCC area is  $\sim 2400$  square degrees,

---

<sup>1</sup>University of Melbourne, School of Physics, Parkville, Victoria 3010, Australia

<sup>2</sup>University of Manchester, Jodrell Bank Observatory, Macclesfield, Cheshire, SK11 9DL, U.K.; vkilborn@jb.man.ac.uk

<sup>3</sup>Australia Telescope National Facility, CSIRO, P.O. Box 76, Epping, NSW 1710, Australia

<sup>4</sup>University of Wales, Cardiff, Department of Physics & Astronomy, P.O. Box 913, Cardiff CF24 3YB, U.K.

<sup>5</sup>Swinburne University of Technology, Mail number 31, PO Box 218, Hawthorn, Victoria 3122, Australia

<sup>6</sup>University of Western Sydney Macarthur, Department of Physics, P.O. Box 555, Campbelltown, NSW 2560, Australia

<sup>7</sup>Department of Physics, University of Bristol, Tyndall Avenue, Bristol, BS8 1TL, U.K.

<sup>8</sup>Research School of Astronomy and Astrophysics, ANU, Weston Creek P.O., Weston, ACT 2611, Australia.

<sup>9</sup>University of New Mexico, Department of Physics & Astronomy, 800 Yale Blvd. NE, Albuquerque, NM 87131, USA

<sup>10</sup>Anglo-Australian Observatory, P.O. Box 296, Epping, NSW 1710, Australia

<sup>11</sup>WIYN Consortium, Inc., 950 N. Cherry Ave. Tucson, AZ, 85726, USA

<sup>12</sup>Astron, PO Box 2, 7990 AA Dwingeloo, The Netherlands

<sup>13</sup>Osservatorio Astronomico di Capodimonte, Via Moiariello 16, 80131 Napoli, Italia

<sup>14</sup>Center for Astrophysics and Space Astronomy, University of Colorado, Boulder, 80309-0389, USA

<sup>15</sup>University of Sydney, Astrophysics Department, School of Physics, A28, Sydney, NSW 2006, Australia

<sup>16</sup>Department of Physics & Astronomy, University of Leicester, Leicester, LE1 7RH, U.K.

<sup>17</sup>Visiting Astronomer, Cerro Tololo Inter-American Observatory, National Optical Astronomy Observatories, which is operated by the Association of Universities for Research in Astronomy, Inc. (AURA) under cooperative agreement with the National Science Foundation.

and covers  $\delta < -62^\circ$ . The average RMS noise for the survey is  $13 \text{ mJy beam}^{-1}$ . Five hundred and thirty-six galaxies have been catalogued according to their neutral hydrogen content, including 114 galaxies that have no previous catalogued optical counterpart. This is the largest sample of galaxies from a blind H I survey to date. Most galaxies in optically unobscured regions of sky have a visible optical counterpart, however there is a small population of low-velocity H I clouds without visible optical counterparts whose origins and significance are unclear. The RMS accuracy of the HiPASS positions is found to be 1.9 arcminutes. The H I-mass range of galaxies detected is from  $\sim 10^6 M_\odot$  to  $\sim 10^{11} M_\odot$ . There are a large number of late-type spirals in the SCC sample (66%), compared with 30% for optically-selected galaxies from the same region in the NASA Extragalactic Database. The average ratio of H I mass to B luminosity of the sample increases according to optical type, from  $1.8 M_\odot/L_\odot$  for early types to  $3.2 M_\odot/L_\odot$  for late-type galaxies. The H I-detected galaxies tend to follow the large-scale structure traced by galaxies found in optical surveys. From the number of galaxies detected in this region of sky, we predict the full HiPASS catalogue will contain  $\sim 5000$  galaxies, to a peak flux density limit of  $\sim 39 \text{ mJy}$  ( $3 \sigma$ ), although this may be a conservative estimate as two large voids are present in the region. The H I mass function for this catalogue is presented in a subsequent paper.

*Subject headings:* galaxies:general; surveys; catalogs

## 1. Introduction

Galaxy evolution is largely driven by the gravitational collapse of overdense regions, and the conversion of gas into stars. At the present epoch, much gas has already been converted into stellar material, although significant quantities remain in the interstellar and intergalactic medium. The largest amount is probably ionised and locked up in the diffuse and warm-hot phases of the intergalactic medium (Davé et al. 2001). However, the cooler, neutral component can more easily condense into stars and galaxies. A direct way of measuring the remaining neutral component, irrespective of the brightness of any accompanying starlight, is through detection of the 21-cm H I line. The H I line is able to reveal primordial gas clouds yet to condense into stars, gas associated with star-forming galaxies, as well as gas resulting from the photodissociation of molecular hydrogen in regions of intense UV radiation (Smith et al. 2000; Allen 2001).

The H I content of galaxies depends to a degree on the environment in which the galaxy resides (Haynes et al. 1984). Galaxies near the centre of clusters are likely to be H I deficient (Solanes et al. 2001; Giovanalli & Haynes 1985), while gas removal effects are not as acute in low density regions and smaller galaxy groups (Huchtmeier et al. 1997; Valluri & Jog 1991). The H I content of galaxies also varies according to their Hubble type. H I is predominately found in spiral galaxies (Rao & Briggs 1993; Hoffman et al. 1989), and Solanes et al. (1996) found that Sb galaxies generally

had a higher H I mass compared to other spirals. The H I content of dwarf galaxies varies with their morphology. Low-luminosity irregular dwarfs are typically H I-rich, while dwarf spheroidal and elliptical galaxies are rarely detected in neutral hydrogen (Carignan 1999; Kraan-Korteweg & Tamman 1979). Low surface brightness (LSB) galaxies are typically H I-rich, and the H I content of LSB dwarf galaxies increases with decreasing optical luminosity (Staveley-Smith et al. 1992). The H I content of E and S0 galaxies is low, with only 10–15% of these galaxies typically detected in neutral hydrogen. It is commonly thought that the majority of the H I seen in these galaxies is from recent or past accretion from a gas-rich companion, as the H I distribution is typically irregular (Duprie & Schneider 1996). However, there is evidence of a small population of low-luminosity early type galaxies and dwarf ellipticals that have an intrinsic content of neutral hydrogen (Oosterloo & Morganti 2000; Sadler 1997), suggesting these galaxies had a different evolutionary path to more luminous, H I poor ellipticals.

The neutral hydrogen (H I) content of the local Universe has hitherto largely been determined using H I observations based on optical or infra-red catalogues of galaxies. However, optical catalogues are biased against galaxies of low optical surface brightness (Impey & Bothun 1997; Disney 1976), so that a substantial part of the possibly H I-rich galaxy population is missed in such surveys. To obtain a thorough census of the neutral hydrogen in the local Universe, blind H I surveys are necessary. Although previous blind H I surveys have covered a range of large-scale structure, the total area surveyed so far is low. The most recent, and largest, blind surveys by Sorar (1994), Spitzak & Schneider (1998) and Rosenberg & Schneider (2000) looked at a range of Right Ascension at particular Declinations, thus enabling a variety of environments to be probed. The number statistics are low, with 65, 75 and 265 galaxies detected respectively. The galaxies follow the same large-scale structure as galaxies detected optically in the same regions. Sorar (1994) and Spitzak & Schneider (1998) found optical counterparts to all their H I detections, and Rosenberg & Schneider (2000) find that most of their detections have an optical counterpart, although some are of very low surface brightness. In addition, blind H I surveys have been conducted through the optically obscured ‘Zone of Avoidance’ (ZOA) (Henning et al. 2000). Such surveys are important in determining the local large-scale structure, which is impossible to do optically in this region (Juraszek et al. 2000). Including these recent ZOA surveys, no population of galaxies has been detected in H I that has significantly increased the calculated H I mass density of the local Universe.

The distribution of H I in the local Universe will soon be known better than ever before, due to the completion of the largest ever survey for H I, the H I Parkes All-Sky Survey (HiPASS). HiPASS has produced some exciting results even in the early stages of analysis, including the discovery of ten new members of the Centaurus A Group (Banks et al. 1999), an H I cloud at low velocity (Kilborn et al. 2000), and an H I cloud associated with NGC 2442 (Ryder et al. 2001). This paper describes the first catalogue produced from  $\sim 11\%$  of the HiPASS survey region. This region covers an area of  $2400 \text{ deg}^2$  in the Southern Celestial Cap (SCC). The catalogue contains 536 galaxies, ranging in mass from  $M_{\text{HI}} \sim 10^6 M_{\odot}$  to  $M_{\text{HI}} \sim 10^{11} M_{\odot}$  ( $H_0$  of  $75 \text{ km s}^{-1} \text{ Mpc}^{-1}$  is assumed throughout). While recent surveys have been concentrating on increasing the

number statistics of low-mass galaxies, this sample occupies a large volume which also enables the increase of statistics on high-mass galaxies. The mass limit of the survey is approximately  $M_{\text{HI}} \sim 10^6 D_{\text{Mpc}}^2 M_{\odot}$ , assuming a line-width of  $100 \text{ km s}^{-1}$ , so the lowest mass galaxies lie within a few Mpc. The catalogue contains 16 galaxies of low H I mass ( $M_{\text{HI}} \lesssim 10^8 M_{\odot}$ ), and 7 galaxies with an H I mass larger than  $3 \times 10^{10} M_{\odot}$ . Higher resolution H I observations were made for a number of detections. These observations as well as the general properties of the sample will be discussed in this paper.

The survey parameters are given in § 2, and the catalogue and selection criteria are described in § 3. The accuracies of the HiPASS derived parameters are explored in § 4. The completeness and reliability of the sample are discussed in § 5. The characteristics of galaxies detected in the survey are presented in § 6, and the spatial distribution is compared to optically known large-scale structure in § 7. The properties of the new H I galaxies are explored in § 8, and finally a summary and predictions for the full survey are presented in § 9. Throughout the paper, the quoted velocities are heliocentric velocities ( $cz$ ), unless otherwise indicated.

## 2. Survey Parameters

HiPASS surveyed the whole Southern sky in H I to Declination  $\delta < +2^\circ$ , and is presently continuing to the North, to  $\delta < +25^\circ$ . A complimentary survey, the H I Jodrell All Sky Survey (HIJASS) is continuing northwards from  $\delta > +25^\circ$  (Boyce et al. 2001). The HiPASS survey uses the Multibeam 13-beam receiver mounted on the Parkes telescope<sup>18</sup>. A 64-MHz bandpass with 1024 channels is used, which gives velocity coverage from  $-1200 \text{ km s}^{-1}$  to  $12,700 \text{ km s}^{-1}$ . The data are bandpass-corrected and gridded into  $8^\circ \times 8^\circ$  cubes (Barnes et al. 2001; Barnes 1998). Once the data are cubed, a further bandpass removal algorithm, LUTHER (Barnes et al. 2001), is run on each of the cubes. This algorithm makes a polynomial fit to the continuum sources in a data cube, then subtracts this template from each of the spectra in the gridded cube, which results in a cube where the flux from continuum sources is minimised. The velocity resolution is  $18 \text{ km s}^{-1}$ , but the channel separation after cubing is  $13.2 \text{ km s}^{-1}$ . The RMS noise level in the final cubes is  $\sim 13 \text{ mJy beam}^{-1}$ . An example of the data quality can be seen in Figure 1. This figure shows a Position-Velocity diagram of part of a HiPASS cube. Galactic emission is seen at  $\sim 0 \text{ km s}^{-1}$ , and the galaxy ESO 099-G 005 is obvious at  $\sim 3600 \text{ km s}^{-1}$ .

The region of sky catalogued for this paper was the South Celestial Cap (SCC) region of the sky,  $\delta < -62^\circ$ . This was one of the first regions of the sky to be completed to the full sensitivity of HiPASS. The SCC region comprises 45 HiPASS cubes, and represents  $\sim 11\%$  of the HiPASS survey. The solid angle covered in the region is 0.74 steradians, and the total volume covered over

---

<sup>18</sup>The Parkes telescope is part of the Australia Telescope which is funded by the Commonwealth of Australia for operation as a National Facility managed by CSIRO.

the full velocity range is  $\sim 10^6$  Mpc<sup>3</sup>.

### 3. The Catalogue

A catalogue of H I–selected galaxies was compiled from the South Celestial Cap (SCC) region of the sky,  $\delta < -62^\circ$ . The catalogue contains 536 galaxies, and 114 of these (21%) have no previous optical identification. In addition, new redshifts were determined for 134 previously catalogued optical galaxies. All galaxies found in the SCC region have a positive radial velocity, even though the negative velocities were searched for galaxies.

Each candidate galaxy was checked in the NASA/IPAC Extragalactic Database<sup>19</sup> (NED) for a known optical counterpart. Optical images for all of the galaxies were obtained from the First Generation Digital Sky Survey<sup>20</sup> (DSS I); for those with no optical counterpart in the First Generation Survey, the image from the Second Generation Digital Sky Survey (DSS II) was obtained. As the beam size of the survey is large, there is the possibility for confusion as to the optical counterpart to an H I detection where there is no available optical redshift. In the case where an optical redshift was not available, the nearest catalogued optical galaxy is suggested as the counterpart to the H I detection. Optical redshifts, or H I synthesis observations will be needed in the future to confirm these optical counterparts. A small number of new detections lie at low velocities in optically unobscured regions, yet do not have obvious optical counterparts in either of the DSS images. One of these detections, HiPASS J1712–64, has been studied in detail, but the nature and formation of this cloud is still uncertain (Kilborn et al. 2000). The nature of these new H I clouds will be discussed in a subsequent paper.

#### 3.1. Galaxy Selection

The catalogue was produced as follows. The candidate galaxy list was formed by visually searching the data cubes. The visual display program, KVIEW (Gooch 1995) was used to search through the data in three dimensions by displaying the data in 2 axes and stepping through the third. Narrow line–width, bright galaxies were most easily seen when the data–cube was displayed in R.A. versus Dec. and stepped through velocity. Large line–width, faint galaxies were more easily discovered when the data–cube was displayed as R.A. or Dec. versus velocity.

It was necessary to impose selection criteria when cataloguing the galaxies, in order to generate a consistent list of H I detections. The selection criteria for this visual sample were that a detection

---

<sup>19</sup>The NASA/IPAC Extragalactic Database (NED) is operated by the Jet Propulsion Laboratory, California Institute of Technology, under contract with the National Aeronautics and Space Administration.

<sup>20</sup>The Digitised Sky Survey, provided by the Space Science Institute, based on photographic data from the UK Schmidt Telescope.

must: (1) be easily visible above the local noise ( $\sim 3\sigma$ ), (2) have spatial extent either greater than or equal to the beamsize (to exclude interference), and (3) be visible over two or more velocity channels. Negative velocity regions were searched, but the heliocentric velocity range from  $-100 \text{ km s}^{-1} \lesssim V \lesssim 200 \text{ km s}^{-1}$  was not searched for galaxies due to confusion caused by Galactic H I emission. The Large and Small Magellanic Clouds and Magellanic Stream and Leading Arm were also excluded from the search region, in the following spatial and velocity ranges. The Large Magellanic Cloud (LMC) lies at R.A. =  $05^{\text{h}}23^{\text{m}}$ , Dec. =  $-69^{\circ}45'$  (J2000), at a heliocentric velocity of  $278 \text{ km s}^{-1}$ . It has an H I line-width of  $\sim 150 \text{ km s}^{-1}$ , and a spatial extent of  $\sim 15^{\circ} \times 13^{\circ}$ . The Small Magellanic Cloud (SMC) lies at R.A. =  $00^{\text{h}}52^{\text{m}}$ , Dec. =  $-72^{\circ}49'$  (J2000), at a heliocentric velocity of  $158 \text{ km s}^{-1}$ . The SMC has an H I line-width of  $\sim 130 \text{ km s}^{-1}$ , and a spatial extent of  $\sim 7^{\circ} \times 4^{\circ}$ . The Magellanic Stream, Leading Arm and associated emission is present in the SCC region, between a heliocentric velocity of  $\sim +80 \text{ km s}^{-1}$  and  $\sim +400 \text{ km s}^{-1}$  (see Putman et al. (1998)). Some regions obviously contained high velocity clouds (HVCs; see Wakker & van Woerden (1991) for a review of HVC properties), consisting of a continuous distribution of resolved, narrow width objects, with  $V \lesssim 450 \text{ km s}^{-1}$ ; these regions were not searched for galaxies due to the high probability of confusion (see Putman et al. (2002) for a catalogue of HVCs in the region). Any detection that was found in the HVC velocity range but which was isolated and had no other HVCs in the same cube was catalogued as a possible galaxy. Therefore six of the detections included in the sample with low radial velocity have ambiguous identities as to their status as an HVC or galaxy. In addition it is likely that some nearby galaxies are not included in the catalogue if their H I emission lies near that of the HVCs. Higher spatial and velocity resolution observations will be needed to distinguish such galaxies from Galactic and HVC H I emission.

To supplement the pure visual examination of the cubes, some objects were added to the catalogue as a result of running automated galaxy finding algorithms through the data. These finders, MultiFind by Kilborn (2001) and a wavelet-based finder by Howlett (*private communication*), are in a preliminary state of readiness, but produced an additional set of objects, 41 of which were confirmed by visual examination and satisfied the same criteria as described above. Mostly these were faint objects with a peak flux  $\lesssim 5\sigma$ , or objects mistakenly missed in the visual search. Their inclusion increases the numbers of faint galaxies available for study, although as discussed later (Section 5 and Kilborn (2002)), it does not make the present catalogue complete at low flux density levels.

### 3.2. Parameterization and Classification of the Galaxies

For each of the detections, the parameters such as flux density, heliocentric velocity and line-width were measured in a semi-automated manner. A script was developed to step through the fitting process, accepting user input at each stage. Using a semi-automated script ensures that the measurements are consistent, yet the user input allowed for reality checks as the measurements were made. MIRIAD routines were used at each step in the fitting process.

Firstly, a two-dimensional Gaussian fit (IMFIT) was made to a velocity-integrated map of each detection in order to determine the central position of the galaxy as well as the spatial extent of the H I. The central position was then used to generate a spatially-integrated spectrum of the detection, using a box size based on the extent of the H I. The spectrum was generated using MBSPECT, which gave a measurement of the peak and integrated flux of each detection, as well as the 50% and 20% velocity width, RMS noise and heliocentric velocity. The heliocentric velocity was measured as the central velocity at the 20% velocity width.

The Local Group correction for the radial velocities used in this paper is

$$V_{LG} = V + 300 \sin l \cos b \quad (1)$$

where  $V_{LG}$  is the Local Group velocity,  $V$  is the heliocentric velocity in optical convention, and  $l$  and  $b$  are the Galactic longitude and latitude. At low velocities, especially where  $V < 500 \text{ km s}^{-1}$ , the distance that can be derived from these corrected velocities is only an estimate due to peculiar motions arising from gravitational interactions with other galaxies.

The galaxies in the SCC sample have been classified according to their optical morphology. The classification followed the scheme described in “The Carnegie Atlas of Galaxies” (Sandage & Bedke 1994). Classifications of previously catalogued optical galaxies were taken from the NED database. It is possible that incorrect or misleading classifications have been made with galaxies of small optical angular extent due to the poor resolution of the DSS I images. Thus the optical types have been divided into four broad classes for analysis - Early Types (E/S0), Early Spirals (Sa-b), Late Spirals (Sc-d), and Late Types (Sm, Im, Irr/pec and dwarf), ignoring any bars. In addition, a number of galaxies could not be classified due to optical obscuration from the Galactic plane. The final problem for optical classification of galaxies was possible confusion in the Parkes beam. Galaxies were flagged if the optical counterpart was confused or interacting, or if an optical identification was not possible. A galaxy was labelled as confused if there was more than one optical galaxy either of unknown redshift or with the same known redshift as the H I detection, within a five arcminute radius of the HiPASS position.

Table 1 is the SCC catalogue of galaxies with derived H I fluxes, and optical properties where available [The complete version of this table is in the electronic edition of the Journal. The printed edition contains only a sample]. The columns in the table are as follows:

(1) HiPASS Name; (2) Right Ascension (J2000); (3) Declination (J2000); (4) Heliocentric Velocity, determined as the center of the 20% velocity width from MBSPECT ( $\text{km s}^{-1}$ ); (5) 20% Velocity width ( $\text{km s}^{-1}$ ); (6) 50% Velocity width ( $\text{km s}^{-1}$ ); (7) Peak Flux Density (Jy); (8) Total Flux ( $\text{Jy km s}^{-1}$ ); (9)  $\log M_{\text{HI}} M_{\odot}$  ( $V_{LG}$  corrected as in Equation 1); (10) Previously catalogued optical name (if exists); (11) Velocity of catalogued optical counterpart; (12) Optical morphology. Galaxies that are confused in their identification are marked with a double dagger on their optical classification. Detections that have been confirmed with further observations are marked with an

asterisk (see Section 5 for details).

#### 4. Accuracy of the derived HiPASS Parameters

The accuracy of the HiPASS parameter values has been tested using two methods. Firstly, high resolution synthesis observations are compared to the HiPASS derived values, then the HiPASS derived fluxes are compared with those of published catalogues.

Follow-up HI synthesis observations were made at the Australia Telescope Compact Array<sup>21</sup> (ATCA). Thirty-seven candidates were observed with the ATCA, using either the 750m or 375m arrays, of which 27 galaxies were detected. Galaxies without previous optical identifications, or without obvious optical counterparts, were chosen for these observations. The observations were made using an 8-MHz bandpass with 512 channels, which gave a channel separation of  $3.3 \text{ km s}^{-1}$ , and a FWHM resolution of  $4.0 \text{ km s}^{-1}$  before smoothing. The observations were made in 'snapshot' mode, with typically 5–6 cuts giving total integration time of  $\sim 3$  hours. The data were reduced using the MIRIAD data reduction package. A secondary calibrator was observed with each galaxy to calibrate the phase, and the primary calibrator, PKS 1934–638 was used to set the primary flux density scale. The data were edited and calibrated, and the bandpass was removed. Bright continuum sources were removed by fitting and subtracting straight lines to the line-free channels in the visibility domain using the MIRIAD task UVLIN. The data were then cubed using natural weighting so as to give the source the highest signal-to-noise possible. The cubes were CLEANed until the absolute maximum residual fell below 3 times the theoretical noise for the cube (typical RMS  $\sim 7 \text{ mJy beam}^{-1}$ ). Finally, the data were RESTORED, and HANNING smoothed.

Table 2 gives the HI derived parameters for the galaxies from the ATCA follow-up observations. The columns are:

(1) HiPASS name; (2) and (3) Central Right Ascension and Declination (J2000) from the ATCA data; (4) Heliocentric velocity ( $\text{km s}^{-1}$ ); (5) and (6) 50% and 20% velocity width, derived from the MIRIAD task, MBSPECT (in  $\text{km s}^{-1}$ ); (7) Peak flux density - derived from the spatially integrated Hanning smoothed spectrum, using MBSPECT (in Jy); (8) Integrated flux - also derived from MBSPECT (in  $\text{Jy km s}^{-1}$ ); (9) Observation month and Year; (10) ATCA array used for the observations.

Ten candidates were not detected in the ATCA observations. Three of the detections had low peak flux densities ( $< 3\sigma$ ). In Parkes confirmation follow-up observations (see section 5), two of these low-flux sources were not re-detected and thus were taken out of the sample, and one was re-detected and therefore kept in the sample. The remaining seven candidates lay well above the HiPASS noise but were resolved out in the ATCA data (all were observed using the 750m array).

---

<sup>21</sup>The Australia Telescope Compact Array is funded by the Commonwealth of Australia for operation as a National Facility managed by CSIRO.



The positional accuracy of the original HiPASS detections is now compared with the follow-up ATCA observations. Figure 2(a) shows the difference in position between the ATCA and HiPASS observations. No correlated offset can be seen between the two sets of H I positions, and the RMS of the scatter for the offset is 1.9 arcmin including both R.A. and Dec. This compares to the predicted range of positional errors from the gridding process of  $\sim 3$  arcmin for a  $3\sigma$  detection to  $\sim 1$  arcmin for a  $10\sigma$  detection (Barnes 1998). The object with the largest ATCA to HiPASS offset (HiPASS J0305–69) is lying on an interference spike in the original HiPASS cube, which hampered the calculation of its centroid position.

Figure 2(b) shows the ATCA and HiPASS measurements for the 50% velocity width. The two measurements agree well for most of the sample. There are two galaxies for which the velocity width determined from HiPASS is higher than the ATCA derived velocity width. HiPASS J1650–62 has a low signal-to-noise ratio, and the difference in measurements appears to be due to noise in the spectrum. The flux detected in the ATCA observations is just 22% of the flux detected in HiPASS, and this appears to have affected the velocity measurement of this galaxy as well. The higher velocity emission was not detected in the ATCA data leading to the conclusion that the higher velocity channels of this galaxy contain extended emission. HiPASS J0908–64 also has a substantial difference between the HiPASS derived  $\Delta V_{50}$  and the ATCA  $\Delta V_{50}$ . This galaxy is a strong source, but the ATCA map indicates some extended emission, and the lower flux emission may have been missed in the ATCA spectrum. In fact, 70% of the HiPASS flux is missed in the ATCA observations. Most of the galaxies had a lower total flux measure from the ATCA observations, as expected due to the incomplete U–V coverage in the synthesis observations. However the full flux was detected for seven of the 27 galaxies. The velocities determined from the ATCA and HiPASS observations matched very well, apart from HiPASS J1650-62 which was previously discussed.

In addition to the synthesis observations, two catalogues have been used to compare and check the fluxes derived from HiPASS. Huchtmeier & Richter (1989) compiled a catalogue of 9500 galaxies. Forty-one galaxies in the SCC sample had entries for total integrated flux in this catalogue. The second comparison catalogue was compiled by Mathewson et al. (1992), who published H I data from pointed observations of 551 galaxies observed with the Parkes Telescope. Thirty-three galaxies from this catalogue were present in the SCC sample. Figure 3 shows a comparison of integrated flux for the overlapping 74 galaxies from both catalogues. The fluxes from the homogeneous Mathewson et al. (1992) catalogue agree very well with the HiPASS derived fluxes, while the heterogeneous Huchtmeier & Richter (1989) fluxes agree to a lesser extent. There is no dependence on the flux ratio with the flux of the galaxies (see Figure 4). The fluxes agree to  $\sim 20\%$  for the Mathewson et al. (1992) comparison and significantly worse for the Huchtmeier & Richter (1989) compilation.

## 5. Completeness and Reliability

Well above the flux density limit, the SCC catalogue is expected to be complete and reliable. However, closer to the flux density limit this situation changes. The approximate  $3\sigma$  flux density detection limit for the catalogue is  $39 \text{ mJy beam}^{-1}$ , however, due to variations in the RMS level for the different cubes, and as the sources were selected largely by visual inspection, the initial catalogue contained sources with peak flux densities down to  $20 \text{ mJy}$ . Figure 5 shows the RMS of each of the cubes in the SCC region, calculated using the AIPS++ STATS routine. This shows, that while the mean RMS is  $\sim 13 \text{ mJy beam}^{-1}$ , the actual RMS of each cube varies from  $9\text{--}17 \text{ mJy beam}^{-1}$  depending on the cube. This means that galaxies in particular cubes are more detectable than others. The main variation arises where the cubes cross the Galactic Plane, as at this position the occurrence of recombination lines is higher, and the number of continuum sources is higher in these regions. Due this RMS variation, a large number of galaxies were catalogued with a peak flux density of less than the average  $3\sigma$  value of  $39 \text{ mJy}$ .

To test the reliability of the catalogue, a selection of sources were re-observed at the Parkes Radiotelescope, using the narrow-band receiver in pointed mode. The sources had a variety of peak flux densities, ranging from  $20 \text{ mJy}$  to over  $200 \text{ mJy}$ . From these confirmation tests, it was found that the reliability of detections with a peak flux density less than the mean  $3\sigma$  ( $39 \text{ mJy}$ ) was poor. Only 50% of the galaxies observed at these low flux densities were re-detected. However, above the  $3\sigma$  limit, the re-detection rate was extremely good. Only one galaxy with a peak flux density of  $41 \text{ mJy}$ , was not re-detected. Due to this, all sources with a peak flux density  $< 39 \text{ mJy}$ , and a number of other sources with a range of peak flux densities, were subsequently re-observed in narrow-band mode at Parkes. About 50% of the candidates were re-detected, and those that were not, were taken out of the catalogue. The catalogue presented in this paper is now expected to contain few false detections, thus the reliability is very high. Figure 6 shows a plot of velocity width versus peak flux density for the sources that were confirmed at Parkes (filled circles), those not confirmed (crosses), and those yet to be observed (open squares). It can be seen that all galaxies re-observed with a peak flux density above  $41 \text{ mJy}$  were re-detected, and there does not seem to be any relationship between the reliability of a detection and its velocity width.

Even though the reliability of this catalogue is high, near the flux density limit, the catalogue is incomplete, meaning that it is most likely missing many weak sources. The completeness of the catalogue is difficult to define particularly as sources were selected largely by visual inspection. Therefore, for statistical purposes, further flux density cuts will be required. Appropriate values for mass function calculation are discussed by Kilborn (2002).

## 6. Characteristics of the Sample

The characteristics of the sample are summarized in Table 3. Galaxies were detected from  $300 \text{ km s}^{-1}$  to  $10610 \text{ km s}^{-1}$ . Below a velocity of  $2000 \text{ km s}^{-1}$  the number of galaxies detected

by HiPASS outnumbered those with already known redshifts from optical surveys. 155 galaxies were detected with a velocity less than  $2000 \text{ km s}^{-1}$  in HiPASS compared with the 112 optically identified galaxies that have known redshifts from the NED database. Of the 112 already known galaxies with redshifts, 82 were re-detected with HiPASS. Thus the total number of galaxies with known redshifts less than  $2000 \text{ km s}^{-1}$  in the SCC region is now 185. The velocity distribution of galaxies in the South Celestial Cap compared with that of all NED<sup>22</sup> galaxies of known velocity in the same region is shown in Figure 7. It is evident that the velocity distribution of HiPASS galaxies does not follow that of optical galaxies in NED. This is expected as the sensitivity limits for optical surveys and HiPASS are different. In addition, HiPASS may not detect nearby clusters of galaxies, due to their deficiency in neutral gas. Solanes et al. (2001) find that two thirds of the clusters they surveyed showed a deficiency of H I near the core which suggests that HiPASS may tend to miss such clusters. So while many optical surveys concentrate on optical clusters, HiPASS may not detect them at all. This effect was most recently seen by Waugh et al. (2002), who looked at HiPASS data of the Fornax cluster and found very few galaxies in the central regions of the cluster. The large beam size of the Parkes telescope also makes the individual detection of galaxies in clusters harder, with the problem rising with increasing distance to the cluster.

The H I mass distribution for the SCC sample is shown in Figure 8(a). The dashed line represents the distribution for the whole sample, and the solid line shows the H I mass distribution of newly detected galaxies. The mass range for the sample is larger than for previous surveys, with the lowest mass galaxy having  $\sim 5 \times 10^6 M_\odot$  of H I and the highest mass galaxy with  $\sim 9 \times 10^{10} M_\odot$  of H I. Most of the H I mass in the sample is contained in galaxies with  $M_{\text{HI}} \sim 10^9 - 10^{10} M_\odot$ . The highest mass galaxy detected in the sample is HiPASS J2123–69, with a velocity of  $10247 \text{ km s}^{-1}$ . There are several optical galaxies visible near the position of this H I detection, so higher resolution H I observations are needed to determine whether the high mass is due to confusion of two galaxies in the Parkes beam. Of the ten most massive galaxies in the sample, only one lies closer than  $6500 \text{ km s}^{-1}$ , and that galaxy is NGC 6744, which lies at a velocity of  $V_{LG} = 715 \text{ km s}^{-1}$ . Synthesis observations of all the most massive galaxies are currently underway at the ATCA, to determine whether these galaxies are single gravitationally bound objects, or several galaxies confused in the Parkes beam. Overall, the H I mass distribution of the new galaxies follows that of the previously catalogued galaxies, although only new galaxies are present in the extreme H I mass bins.

Figure 8(b) shows the distribution of 20% velocity widths ( $\Delta V_{20}$ ) for the sample. The largest velocity width is  $\Delta V_{20} = 770 \text{ km s}^{-1}$ , but this is a confused detection in the Parkes beam comprising the galaxies NGC 6872 and IC 4970. The smallest velocity width galaxy in the sample is HiPASS J1614–72, which has  $\Delta V_{20} = 35 \text{ km s}^{-1}$ , which is just twice the velocity resolution of HiPASS. This detection is one of the confused HVC/dwarf galaxies, and lies at a low systemic velocity. The mean  $\Delta V_{20}$  for the sample is  $\Delta V_{20} = 240 \text{ km s}^{-1}$ , and the mean 50% velocity width for the sample is  $\Delta V_{50} = 186 \text{ km s}^{-1}$ .

---

<sup>22</sup>It is noted that the NED optical catalogue is heterogeneous, so that comparison is difficult.

### 6.1. Optical Properties

The majority of galaxies in the SCC sample are classified as Spirals (309 galaxies, or 68%). There were more late-type spirals than early, with 28% being Sa/Sb and 40% classified as Sc/Sd. The number of S0s in the sample is low, 20 or  $\sim 6\%$ , and there were just two galaxies classified as Elliptical. The majority of the newly detected galaxies that could be optically identified were faint late types. Eighty-eight galaxies could not be optically identified due to either their Galactic obscuration, or the presence of two or more possible optical candidates. Three galaxies were seen to be interacting from their optical images, and 68 galaxies were confused in the Parkes beam.

1398 galaxies with known redshifts have been catalogued optically in the SCC region, according to the NED database. Of these, 793 have morphological classifications from NED. 448 galaxies in the SCC catalogue were able to be morphologically classified. The percentage break down of optical morphology of all optical galaxies in the SCC region with classifications compared to the break-up of optical types of the HiPASS galaxies is shown in Figure 9. The distribution of galaxy type in the optical catalogues is quite different to that in the HiPASS catalogue. The optical catalogues contain a much higher percentage of early-type galaxies (24% optical cf. 6% HiPASS), while the HiPASS catalogue has a much greater number of late-type galaxies (26% HiPASS cf. 4% optical). The percentage of spirals in each sample is similar, but the early spirals dominate the optical sample while the late spirals dominate the HiPASS catalogue.

Figure 10 shows the distribution of H I mass-to-light ratios for the SCC sample. The optical luminosity was determined from the B magnitudes given in the ESO-LV catalogue for the previously catalogued galaxies, or from optical observations from the MSSSO 40 inch telescope (Marquarding 2000) for some of the new HiPASS detections. Most of the galaxies detected with HiPASS have an  $M_{\text{HI}}/L_B < 5$ , but 28 galaxies have a higher  $M_{\text{HI}}/L_B$ . The galaxy with the highest  $M_{\text{HI}}/L_B$  is HiPASS J0019–77, with  $M_{\text{HI}}/L_B = 24$ . This is a previously known ESO galaxy, but the HiPASS observation represents the first H I detection. This particular detection may be confused however, as there are two optical galaxies close by, and only one has a measured redshift. Table 4 gives the  $\langle M_{\text{HI}}/L_B \rangle$  for the different optical morphologies. The mean H I mass-to-light ratios for galaxies of different Hubble type varies from 1.8 for early-types, to 3.2 for late-types. The average value for the early-types in particular is quite high. Within the sample of 10 early-types for which optical information was available, there is only one galaxy with an elliptical classification ( $M_{\text{HI}}/L_B = 0.3$ ), with the rest classified as S0 ( $\langle M_{\text{HI}}/L_B \rangle = 1.9$ ). Half of the S0 galaxies are actually classified as S0 peculiar, possibly indicating an interaction in the past, and this could explain the high value for  $\langle M_{\text{HI}}/L_B \rangle$ . Also two of the S0 galaxies are labelled as confused, and the H I may be associated with nearby Sc galaxies. The early and late spiral galaxies have similar  $\langle M_{\text{HI}}/L_B \rangle$ , but the average value for the early spirals is influenced by the inclusion of HiPASS J0019–77, which has an  $M_{\text{HI}}/L_B$  of 24, which is much higher than the other early spiral galaxies. The median values show an increase in  $M_{\text{HI}}/L_B$  from early to late spiral galaxies.

## 7. Spatial Distribution of the HI Selected Galaxies

The distribution of the HiPASS galaxies on the sky is similar to the distribution of already known galaxies in the region. Figure 11 shows the HiPASS galaxies plotted, with the previously catalogued galaxies with a redshift in the HiPASS detection range. The newly discovered HiPASS galaxies do not fill the voids, and follow the general distribution of the optically catalogued galaxies. The exception is near the Galactic plane, where the catalogue of optical galaxies is incomplete. Several optical clusters can be seen in Figure 11, eg: the PAVO II cluster at  $(l, b) = (332.3, -23.5)$ ,  $V = 4167 \text{ km s}^{-1}$ . This cluster has more than 30 optically classified members, yet only one is detected in HiPASS. The clustering properties and correlation function for this sample is investigated further in Tantisrisuk et al. (2002).

The distribution of HiPASS galaxies for different velocity ranges is now compared to known optical large-scale structure based on maps by Fairall (1998). Figures 12 and 13 show the distribution of HiPASS galaxies: those with previous optical counterparts are indicated by filled circles and galaxies with no previous optical identifications are shown with stars. The Magellanic Clouds are shown by the large unfilled circles on each plot. Major features are noted, and are described below.

The main structure seen at the lowest velocities ( $V < 1000 \text{ km s}^{-1}$ ) is the edge of the Centaurus wall, which runs perpendicular to the Galactic plane at a Galactic longitude of  $\sim 330^\circ$ . A number of new detections were discovered in this region. Mostly they are ambiguous HVC/galaxy detections without visible optical counterparts. The Centaurus wall is an edge-on feature that runs parallel to the Supergalactic plane. This velocity range represents only  $\sim 0.05\%$  of the total volume of the SCC region, but this is the limiting velocity range for finding low-mass galaxies ( $M_{HI} \lesssim 10^8 M_\odot$ ).

Between velocities  $1000 \text{ km s}^{-1}$  and  $1999 \text{ km s}^{-1}$ , the Fornax wall appears: The Fornax cluster lies off the plot in the direction of the top right corner. The Fornax wall is a face-on feature. In the next velocity region ( $2000 \text{ km s}^{-1}$  to  $2999 \text{ km s}^{-1}$ ) a fragment of the Fornax wall is present, and the Eridanus void can be seen to the bottom left of the plot. The structure of galaxies continues moving to the right as we look deeper in velocity, and between velocities of  $3000 \text{ km s}^{-1}$  and  $3999 \text{ km s}^{-1}$  the Pavo spur is quite obvious, and the Eridanus void is still present. There are a number of new galaxies towards the plane of the Galaxy at this velocity, and it is possible we are seeing a new structure that joins the Fornax and Centaurus clusters via the Fornax wall.

The edge of the Centaurus wall is evident again between the velocities of  $4000 \text{ km s}^{-1}$  and  $4999 \text{ km s}^{-1}$ , and the Eridanus void is starting to disappear. The next velocity range,  $5000 \text{ km s}^{-1}$  to  $5999 \text{ km s}^{-1}$ , contains the start of the Sculptor void, along with a several new galaxies towards the plane of the Milky Way.

Due to the sparsity of HiPASS detections above a velocity of  $6000 \text{ km s}^{-1}$ , no large-scale structure has been indicated. In the velocity range  $6000 \text{ km s}^{-1}$  to  $7000 \text{ km s}^{-1}$ , the number of new HiPASS galaxies outnumbers the number of galaxies HiPASS detected with known optical

counterparts. Once again the new galaxies tend to be found towards the plane of the Galaxy. There are still a significant number of new galaxies being detected above a velocity of  $7000 \text{ km s}^{-1}$ , and in this velocity range only large H I mass galaxies have flux limits above the HiPASS sensitivity limit.

## 8. Properties of the Newly Detected Galaxies

One hundred and fourteen galaxies without previous NED identifications were found in the SCC region of sky. The new galaxies mainly consist of optically faint galaxies, compact high surface brightness galaxies, and galaxies optically obscured by the Milky Way. A large H I cloud was detected near the galaxy NGC 2442 which does not seem to have any associated optical emission (Ryder et al. 2001). In addition a number of isolated H I clouds were found at velocities between  $300 \text{ km s}^{-1}$  and  $500 \text{ km s}^{-1}$ , including the H I cloud HiPASS J1712-64 (Kilborn et al. 2000). It is uncertain whether these clouds are extragalactic or whether they are a product of the Magellanic Clouds/Galaxy interaction. A large percentage of the new galaxies lie along the Galactic Plane, although a number of dwarf galaxies were discovered that were not in visually obscured regions. A couple of galaxies were found visually obscured by the Large Magellanic Cloud, which will be important for unbiased measurements of dust extinction in the Clouds (Dutra et al. 2001).

As mentioned in Section 4, a number of these new galaxies have been observed at the ATCA. In general, the galaxies chosen for observation were those with no obvious optical counterpart on the DSS images. Of those galaxies detected with the ATCA, all apart from the previously mentioned HiPASS J1712-64 have optical emission associated with them. Two examples of high surface brightness new detections are shown in Figure 14. HiPASS J0305-69 consists of two H I clumps, with a compact optical counterpart associated with the larger clump. There is another compact optical counterpart for the smaller clump, but it is unclear whether this counterpart is a foreground star, or emission associated with the galaxy. HiPASS J1816-67 has a very large H I disk surrounding the compact optical counterpart. In both these detections the optical counterparts are hardly more extended than the foreground stars, leading to them being missed in previous optical galaxy surveys. Four low-mass LSB galaxies were detected. These galaxies all have a smooth distribution of H I, with a faint optical counterpart lying in the highest column density region of their disks. The disks are typically 2–3 times the spatial size than the visible optical counterpart. The lowest-mass new galaxy detected was HiPASS J1247-77, which has an H I mass of  $4.6 \times 10^6 M_{\odot}$  for an estimated distance of 2.2 Mpc. The ATCA synthesis image overlaid on the DSS I optical image is shown in Figure 15. This galaxy lies close to emission from the Magellanic Clouds, and is also nearby the dwarf galaxy IC 3104, which lies at  $430 \text{ km s}^{-1}$ .

## 9. Summary

The SCC catalogue allows the study of the H I content of galaxies free from any optical bias in the sample selection. The accuracy of HiPASS detections was determined using follow-up observations at the ATCA. The positional RMS from the ATCA observations was 1.9 arcminutes. The H I selected galaxies followed the large-scale structure laid out by optical catalogues, although the number of H I detections in optical regions of high galaxy density was not high. The mass range of the sample is very large – from  $\sim 5 \times 10^6 M_\odot$  to  $\sim 9 \times 10^{10} M_\odot$ , which is the largest mass range from a blind H I survey of galaxies. The size of the catalogue allows for the optical properties of the H I-rich galaxies to be studied. More late-type galaxies were found in the H I sample, with 58% of galaxies being either late spirals or late-types, compared to 30% for the known optically selected galaxies in the same region. The H I mass-to-light ratio increased from a mean value of 1.8 for early type galaxies to 3.2 for late-types. The galaxies are much more gas rich than typical values from optical samples.

Galaxies without previously catalogued optical counterparts generally had either an LSB counterpart nearby, were located near a bright star, or were in the optically obscured ZOA. A small number of H I clouds without optical counterparts was found, but these lay at low velocities, and it is unclear whether these are extragalactic H I clouds or HVCs that are associated with the Magellanic Clouds/Galaxy interaction. From the number of galaxies detected in this region, we predict that the full survey will contain in excess of 5000 galaxies, down to a peak flux limit of 39 mJy. This number is a lower limit, as the presented catalogue is likely to be incomplete at this flux level, and with improved galaxy detection algorithms the final catalogue should be more complete. In addition there were two voids in the SCC region – the Sculptor and Eridanus voids – which has possibly resulted in fewer detections in this region than in HiPASS on average.

## Acknowledgments

We would like to thank the staff at the Parkes observatory for their support throughout the observations, and the ZOA team for help with HiPASS observations. We are grateful to S. Gurovich, S. Mader, J. Stevens and M. Zwaan for providing details about narrow-band confirmation observations. Thanks also to the referee for helpful remarks. V. Kilborn acknowledges support from an Australian Postgraduate Award.

## REFERENCES

- Allen, R. J. 2001, Gas and Galaxy Evolution, ASP conference Proceedings, Vol. 240, eds Hibbard, J. E., Rupen, M. P., & van Gorkom, J. H., p331
- Banks, G. D., Disney, M. J., Knezek, P. M. et al 1999, ApJ, 524, 612

- Barnes, D. G., Staveley-Smith, L., de Blok, W. J. G. et al. 2001, MNRAS, 322,486
- Barnes, D. G. 1998, PhD Thesis, University of Melbourne
- Boyce, P. J., Minchin, R. F., Kilborn, V. A. et al. 2001, ApJL, 560, 127
- Carignan, C. 1999, P.A.S.A., 16, 18
- Davé, R., Renyue, C., Ostriker, J. P. et al. 2001, ApJ 552, 473
- Disney, M. J. 1976, Nature, 263, 573
- Duprie, K. & Schneider, S. E. 1996, ApJ, 112, 937
- Dutra, C. M., Bica, E., Clariá, et al. 2001, A. & A. *accepted*, astro-ph 0103518
- Fairall, A. 1998, *Large Scale Structures in the Universe*, John Wiley & Sons
- Giovanelli, R. & Haynes, M. P. 1985, ApJL 346, L5
- Gooch, R. 1995, ASP Conf. Ser. 77: ADASS IV, Volume 4
- Haynes, M. P., Giovanelli, R. & Chincarini, G. L. 1984, ARA&A, 22, 445
- Henning, P. A., Staveley-Smith, L., Ekers, R. D. et al. 2000, AJ, 119, 2686
- Hoffman, G. L., Williams, B. M., Lewis, B. M. et al. 1989, ApJS, 69, 65
- Huchtmeier, W. & Richter, O. 1989, *A General Catalog of HI Observations of Galaxies*, Springer-Verlag
- Huchtmeier, W. K., Hopp, U. & Kuhn, B. 1997, A&A, 319, 67
- Impey, C. D. & Bothun, G. D. 1997, ARA&A, 35, 267
- Juraszek, S. J., Staveley-Smith, L. Kraan-Korteweg, R. C. et al. 2000, AJ, 119, 1627
- Kilborn, V. A., Staveley-Smith, L., Marquarding, M. et al. 2000, AJ, 120, 1342
- Kilborn, V. A., 2001, PhD Thesis, University of Melbourne
- Kilborn, V. A., et al. 2002 *in preparation*
- Kraan-Korteweg, R. C. & Tammann, G. A. 1979, Astronomische Nachrichten, 300, 181
- Marquarding, M. 2000, Master's Thesis, University of Melbourne
- Mathewson D. S., Ford, V. L. and Buchhorn, M. 1992, ApJS 81, 413
- Oosterloo, T. & Morganti, R. 2000, in *Gas and Galaxy Evolution*, ASP Conference Series 2000, J. E. Hibbard, M. P. Rupen & J. H. van Gorkom, editors



- Putman, M. E., Gibson, B. K., Staveley–Smith, L. et al. 1998, *Nature*, 394, 752
- Putman, M. E. et al. 2002, *AJ*, 123, 873
- Rao, S. & Briggs, F. 1993, *ApJ*, 36, 267
- Rosenberg, J. L. and Schneider, S. E. 2000, *ApJS*, 130, 177
- Ryder, S. D., Koribalski, B., Staveley–Smith, L. et al. 2001, *ApJ*, 555, 232
- Sadler, E. M. 1997, *P.A.S.A.*, 14, 45
- Sandage, A. and Bedke, J. 1994, *The Carnegie Atlas of Galaxies*, Carnegie Institute of Washington
- Smith, D. A., Allen, R. J., Bohlin, R. C. et al. 2000, *ApJ*, 538, 608
- Solanes, J. M., Giovanelli, R. & Haynes, M. P. 1996, *ApJ*, 461, 609
- Solanes, J. M., Manrique, A., Garcia–Gomez, G. and Gonzalez–Casado, G., Giovanelli, R. and Haynes, M. P., 2001, *ApJ*, 548, 97
- Sorar 1994, PhD Thesis, Pittsburgh University
- Spitzak, J. G. and Schneider, S. E. 1998, *ApJS*, 119, 159
- Staveley–Smith, L., Davies, R. D. & Kinman, T. D. 1992, *MNRAS*, 258, 334
- Tantisrisuk et al. 2002, *in preparation*
- Valluri, M. & Jog, C. J. 1991, *ApJ* 374, 103
- Wakker, B. P. & van Woerden, H. 1991, *A. & A.*, 250, 509
- Waugh, M. et al, 2002, *MNRAS*, *submitted*

Dec:  $-64^{\circ} 11' 58.93''$  (J2000)

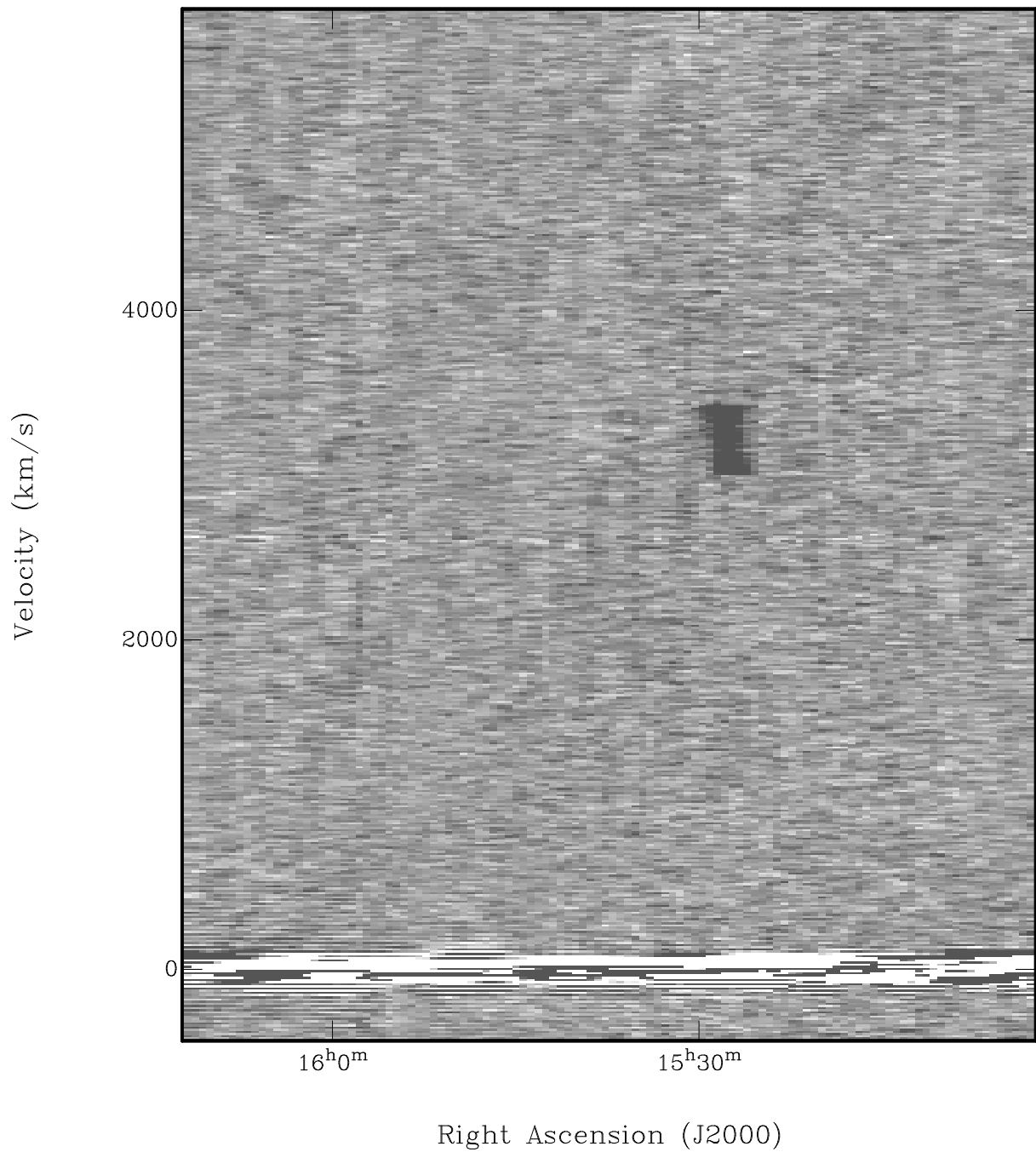


Fig. 1.— A section of a HiPASS data cube at roughly constant Declination. Visible are Galactic H I emission at  $0 \text{ km s}^{-1}$ , and the galaxy ESO 099-G 005 at  $\sim 3600 \text{ km s}^{-1}$ .

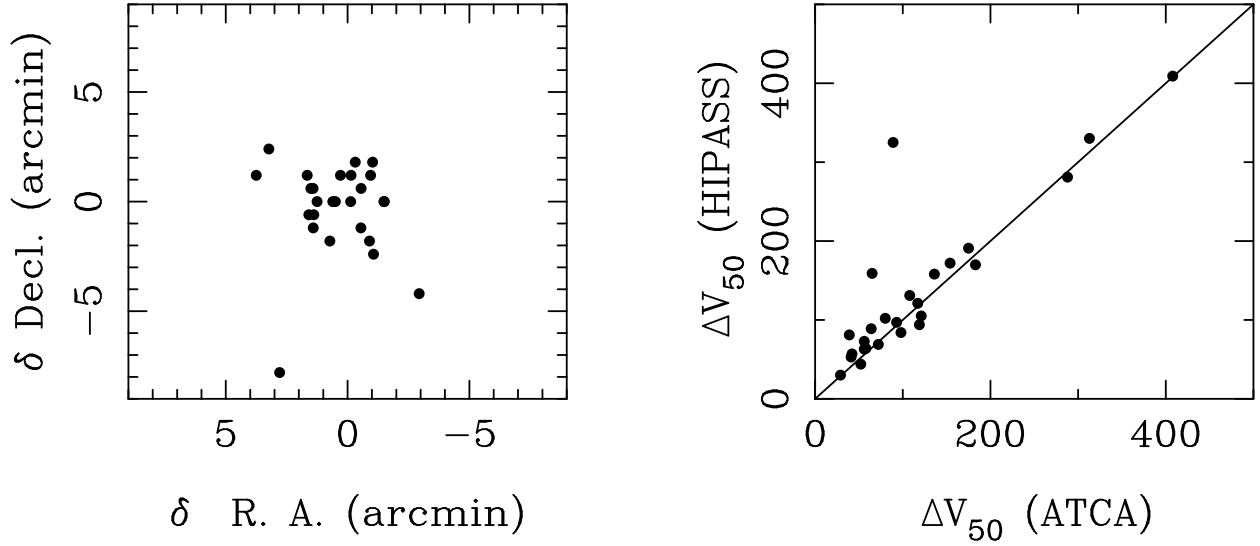


Fig. 2.— (a) Difference in R.A. and Dec. for the ATCA measurements and HiPASS measurements. The RMS of the scatter is 2.1 arcmin for R.A. and 1.7 arcmin for Dec. (b)  $\Delta V_{50}$  from HiPASS versus  $\Delta V_{50}$  from the ATCA. The solid line represents equal velocity width measurements. Two measurements lie faraway from this line due to the ATCA resolving out part of the flux of these galaxies.

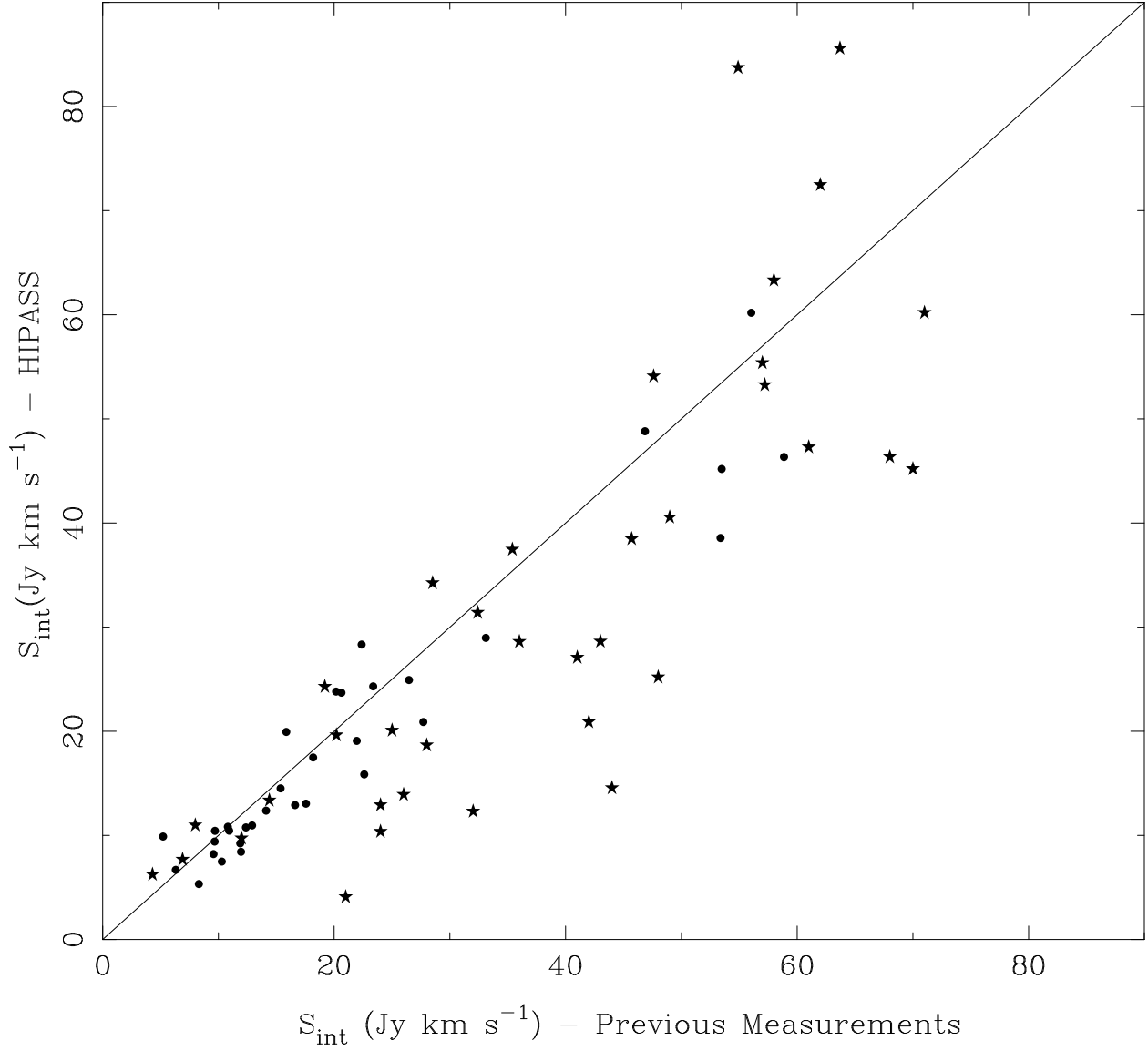


Fig. 3.— Integrated flux measurements from the Huchtmeier & Richter (1989) catalogue (stars) and the Mathewson et al. (1992) catalogue (circles), compared to HiPASS measurements. The Mathewson et al. (1992) measurements compare quite well with HiPASS fluxes, while the Huchtmeier & Richter (1989) tend to be higher. The HiPASS fluxes tend to be lower than the previous measurements.

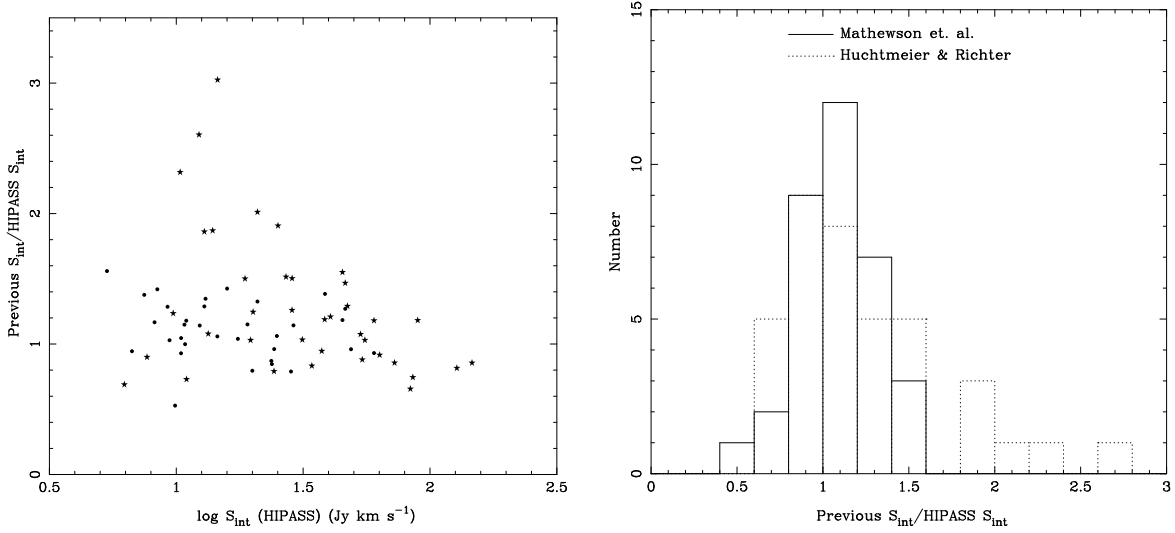


Fig. 4.— [Left] No relationship is seen between the ratio of previous to HiPASS fluxes with integrated flux. The symbols are the same as in Figure 3. [Right] The corresponding histogram of flux ratios. Most of the Mathewson et al. (1992) fluxes agree with the HiPASS fluxes within 20%. The scatter is larger for the Huchtmeier & Richter (1989) fluxes.

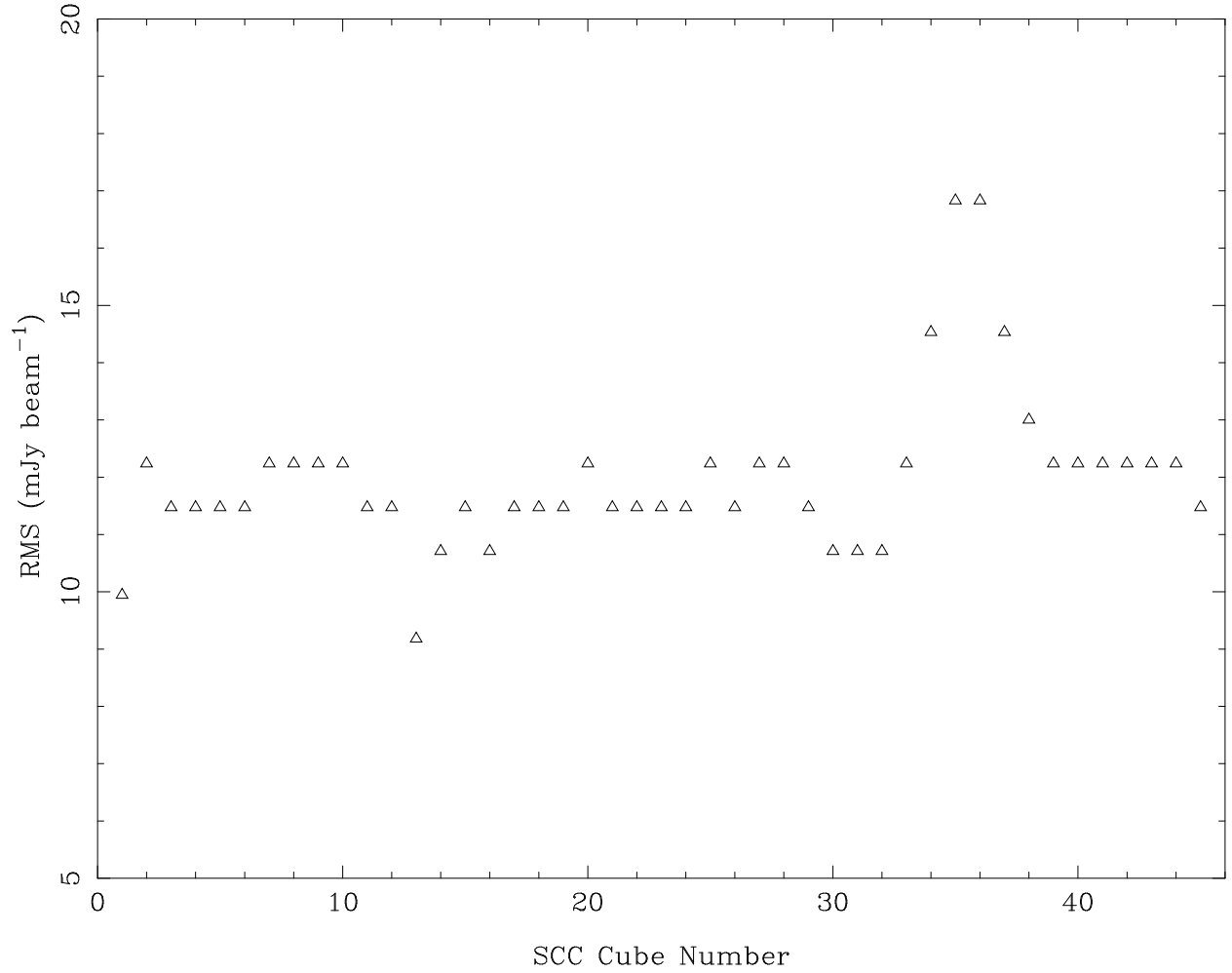


Fig. 5.— RMS noise in SCC cubes. The RMS is higher in cubes that lie near the Galactic Plane. HIPASS cubes are approximately  $8^\circ \times 8^\circ$ . Cube 1 is centred at Dec.  $-90^\circ$ ; cubes 2–9 are centred between R.A. 0h and 24h at Dec.  $-82^\circ$ ; cubes 10–24 are centred between R.A. 0h and 24h at Dec.  $-74^\circ$ , and cubes 25–45 are centred between R.A. 0h and 24h at Dec.  $-66^\circ$ . The quantisation of the RMS values is caused by the 16-bit integer precision that is used in the cubing.

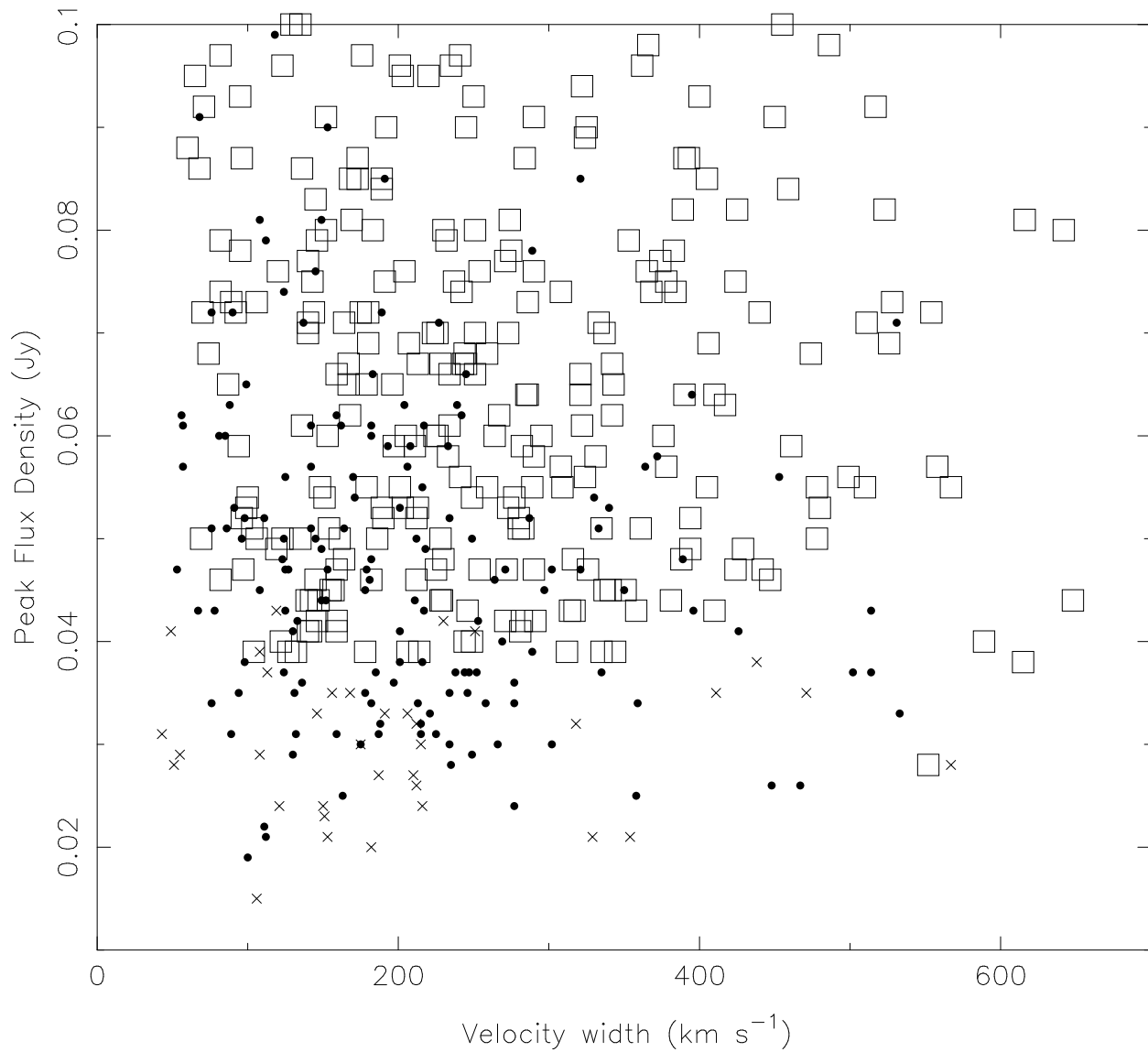


Fig. 6.— Narrow-band confirmation detections. The open squares are galaxies yet to be confirmed, the filled circles are confirmed detections and the crosses are galaxies not re-confirmed in pointed narrow-band observations. Galaxies with lower flux densities tended to be less reliable, and the velocity width of the detection does not seem to correlate with the reliability.

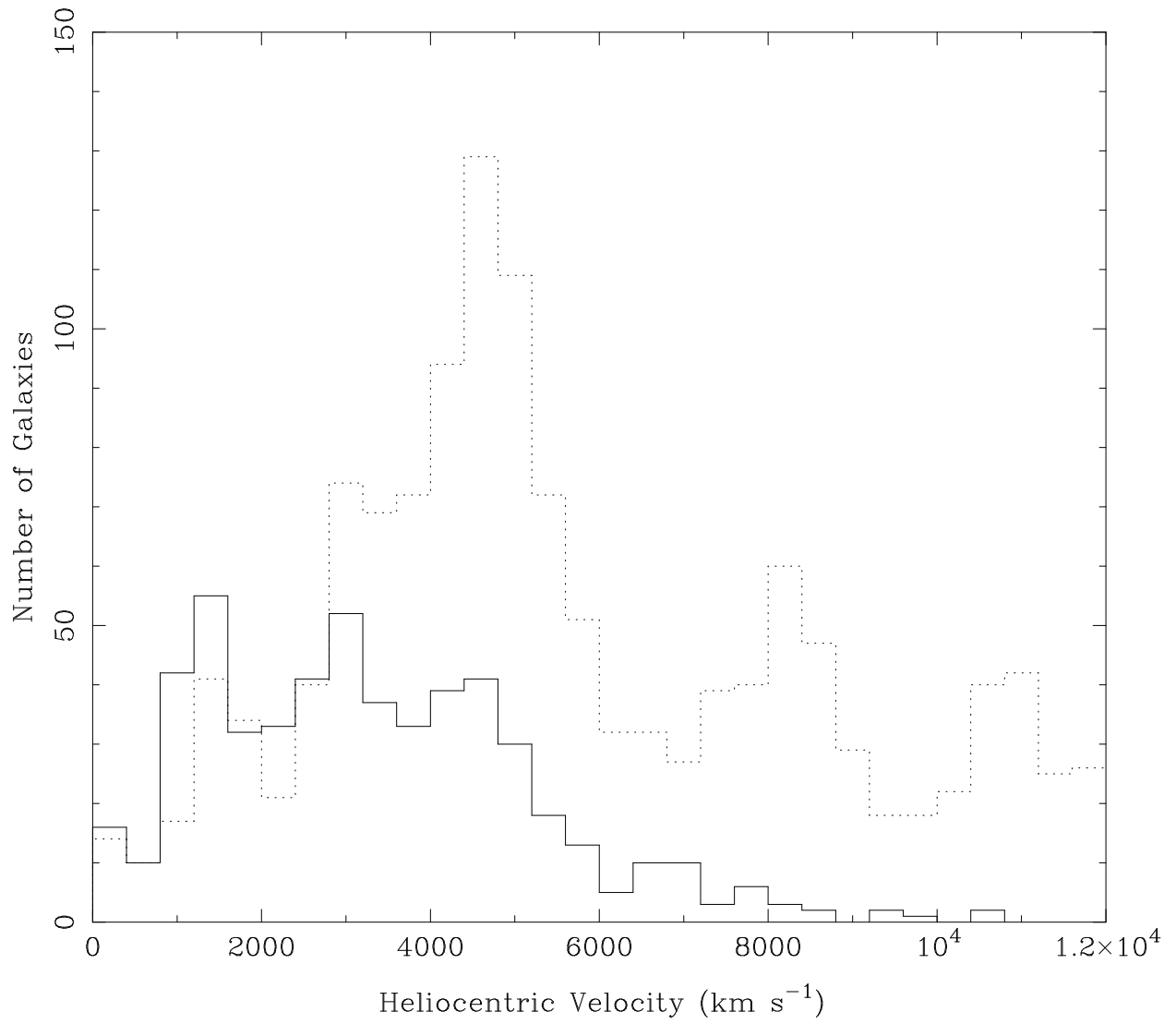


Fig. 7.— Velocity Distribution of the SCC sample (solid line), and all galaxies in the NED database with known redshift (dotted line).



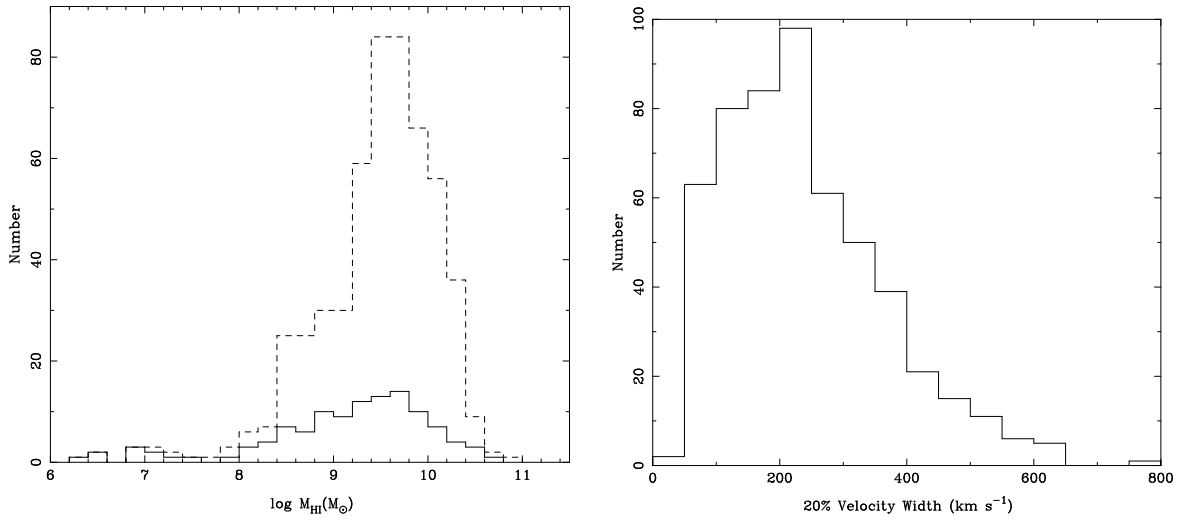


Fig. 8.— (a) H I Mass Distribution for the SCC Sample. The dashed line shows the H I mass distribution for the full sample, and the solid line shows the H I mass distribution of the newly detected galaxies. (b) Distribution of 20% velocity widths for the SCC Sample (not corrected for inclination).

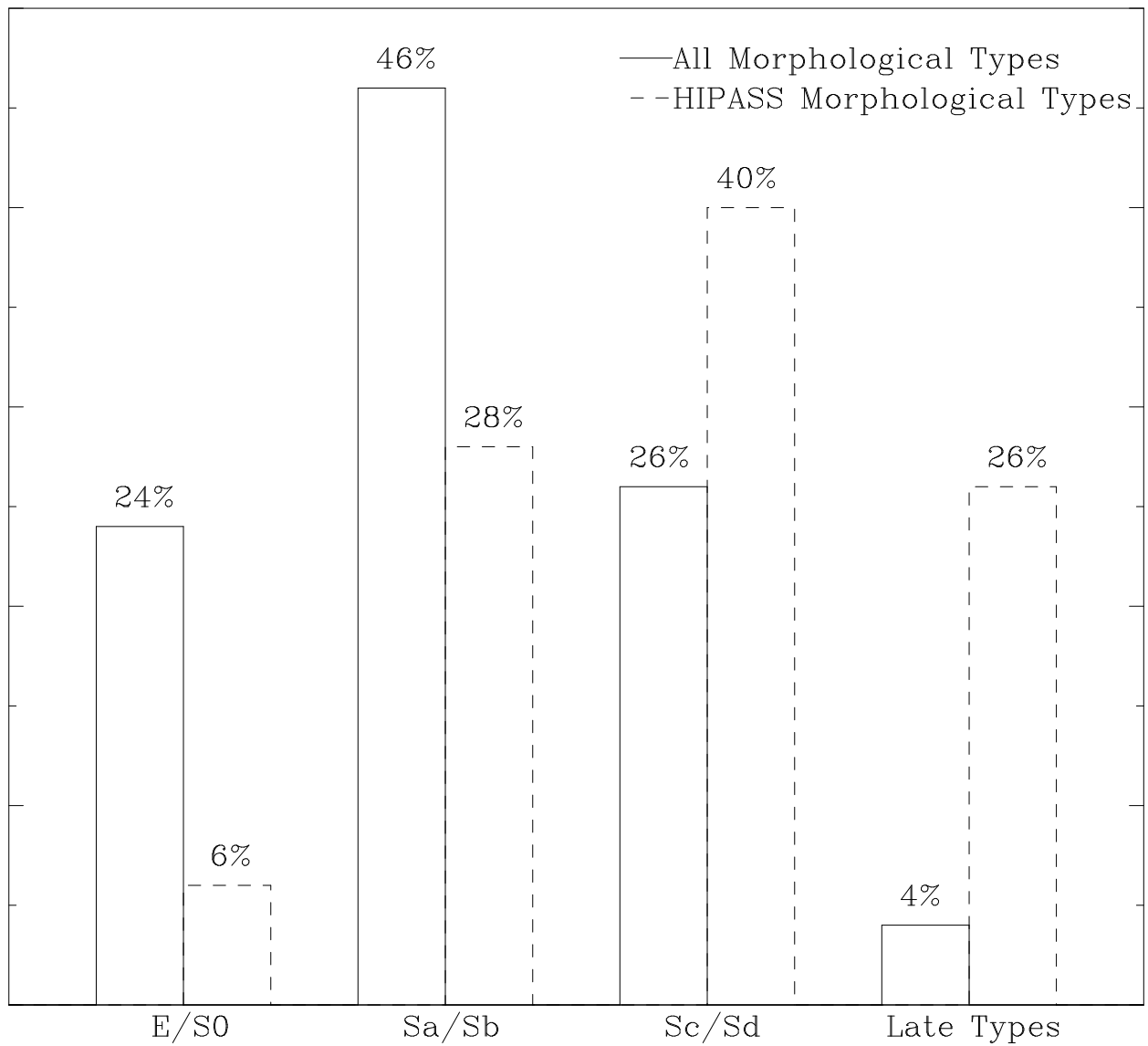


Fig. 9.— Morphological classifications for all optically identified galaxies in the SCC region (solid line), and all HiPASS galaxies in the SCC region (dashed line).

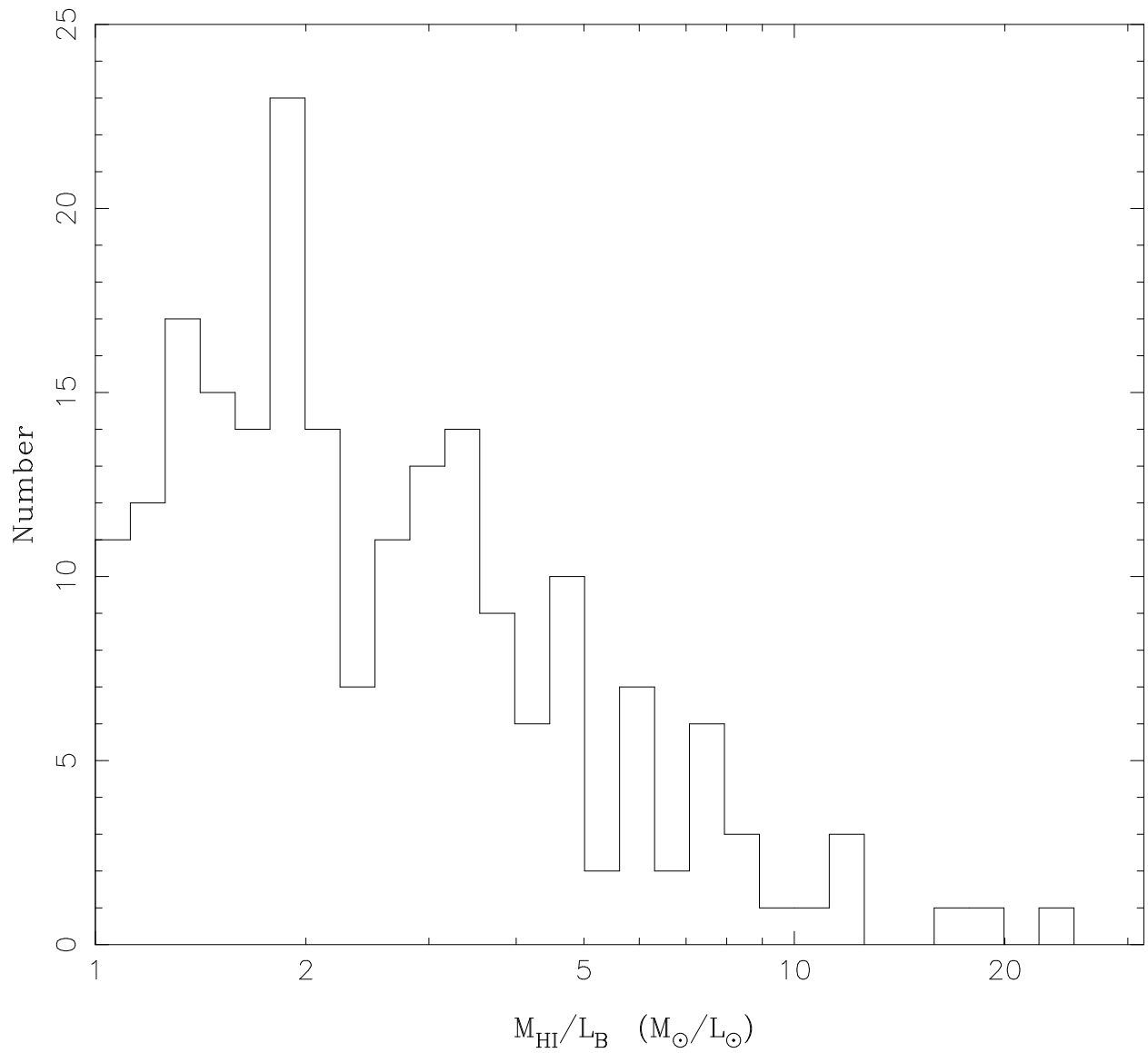


Fig. 10.— Distribution of HI mass-to-light ratios for galaxies with published ESO-LV B-magnitudes.

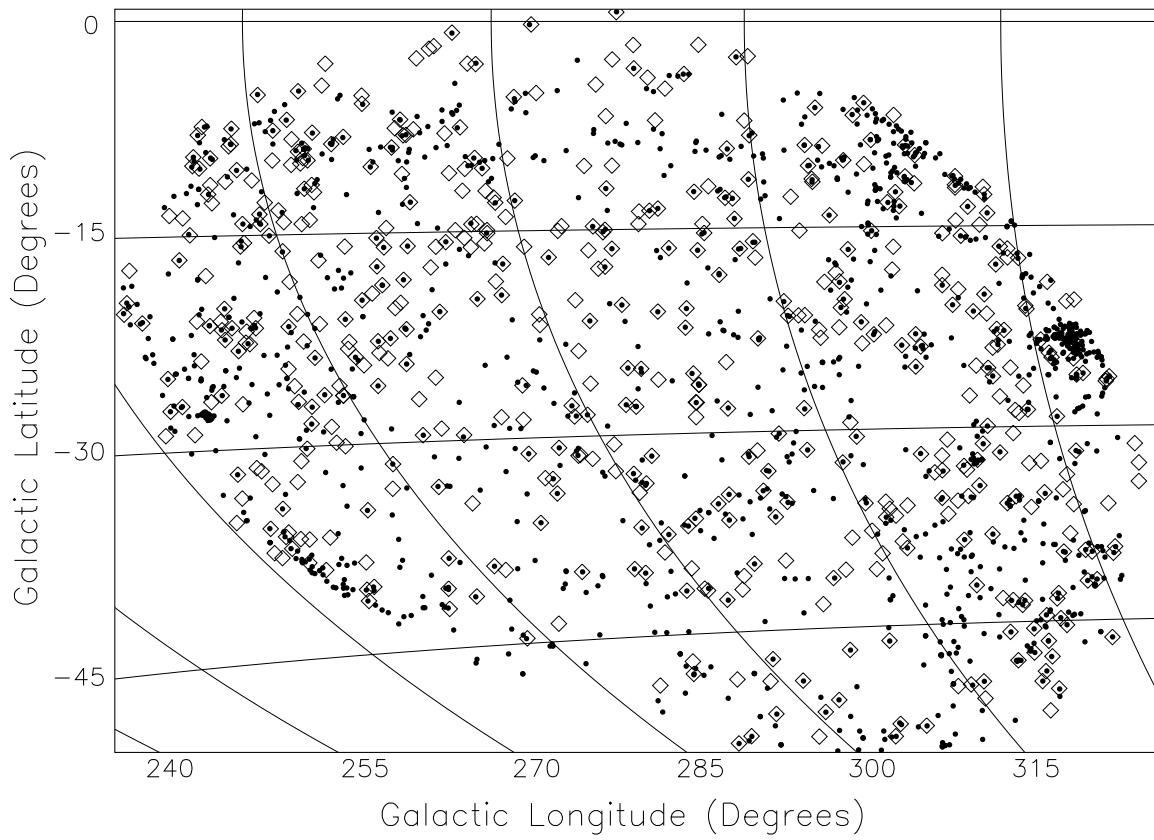


Fig. 11.— Spatial distribution of SCC galaxies. The diamonds show HI-PASS galaxies, and the filled circles show previously catalogued optical galaxies in the same velocity range as the SCC sample.

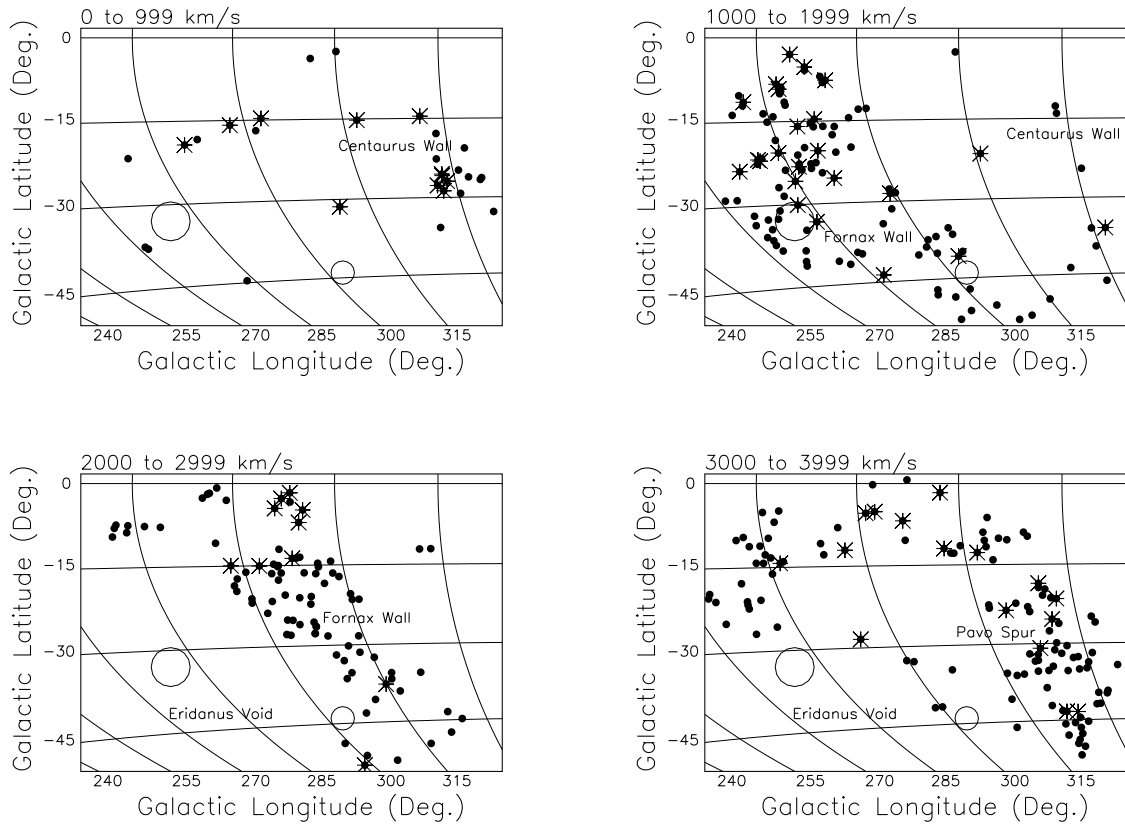


Fig. 12.— Distribution of South Cap galaxies in 4 velocity ranges (I). Filled circles are HiPASS detections with a known optical counterpart, and the stars are new HiPASS detections. The large open circles represent the Magellanic Clouds.

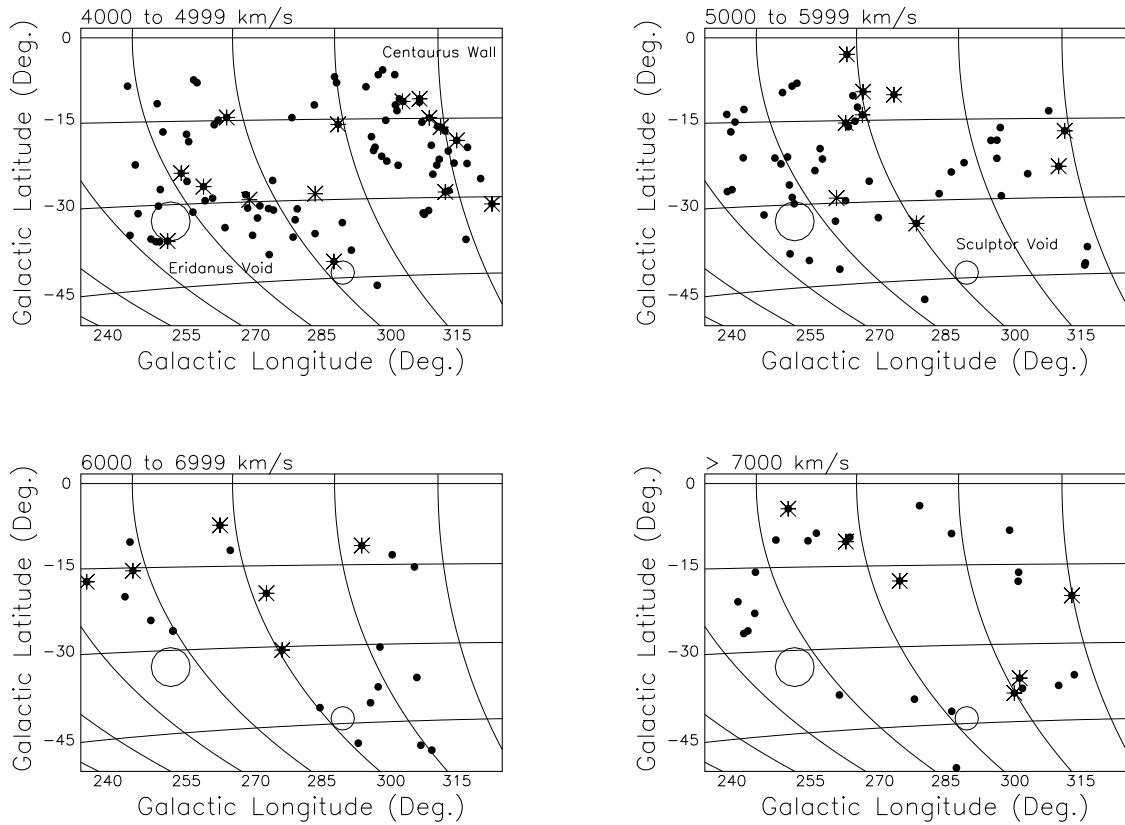


Fig. 13.— Distribution of South Cap galaxies in 4 velocity ranges (II). Filled circles are HI-PASS detections with a known optical counterpart, and the stars are new HI-PASS detections. The large open circles represent the Magellanic Clouds.

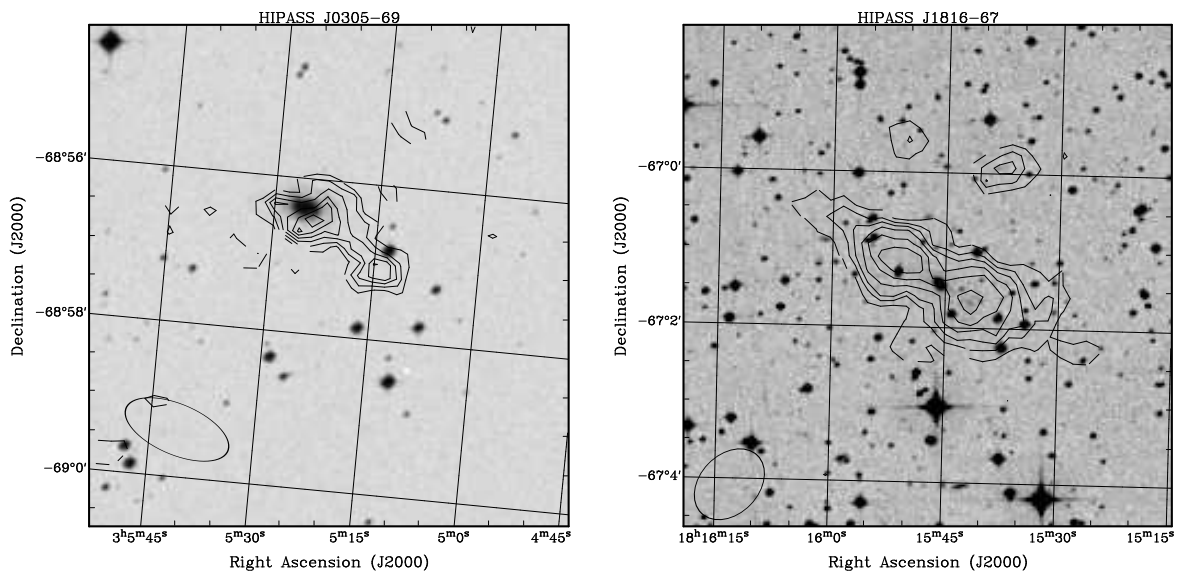


Fig. 14.— ATCA observations of previously uncatalogued high surface brightness galaxies. The ATCA H I contours are overlaid on DSS I images. The optical counterparts are compact, resulting in their being missed in optical surveys. The beam for the H I observations is shown in the bottom left corner of each image.

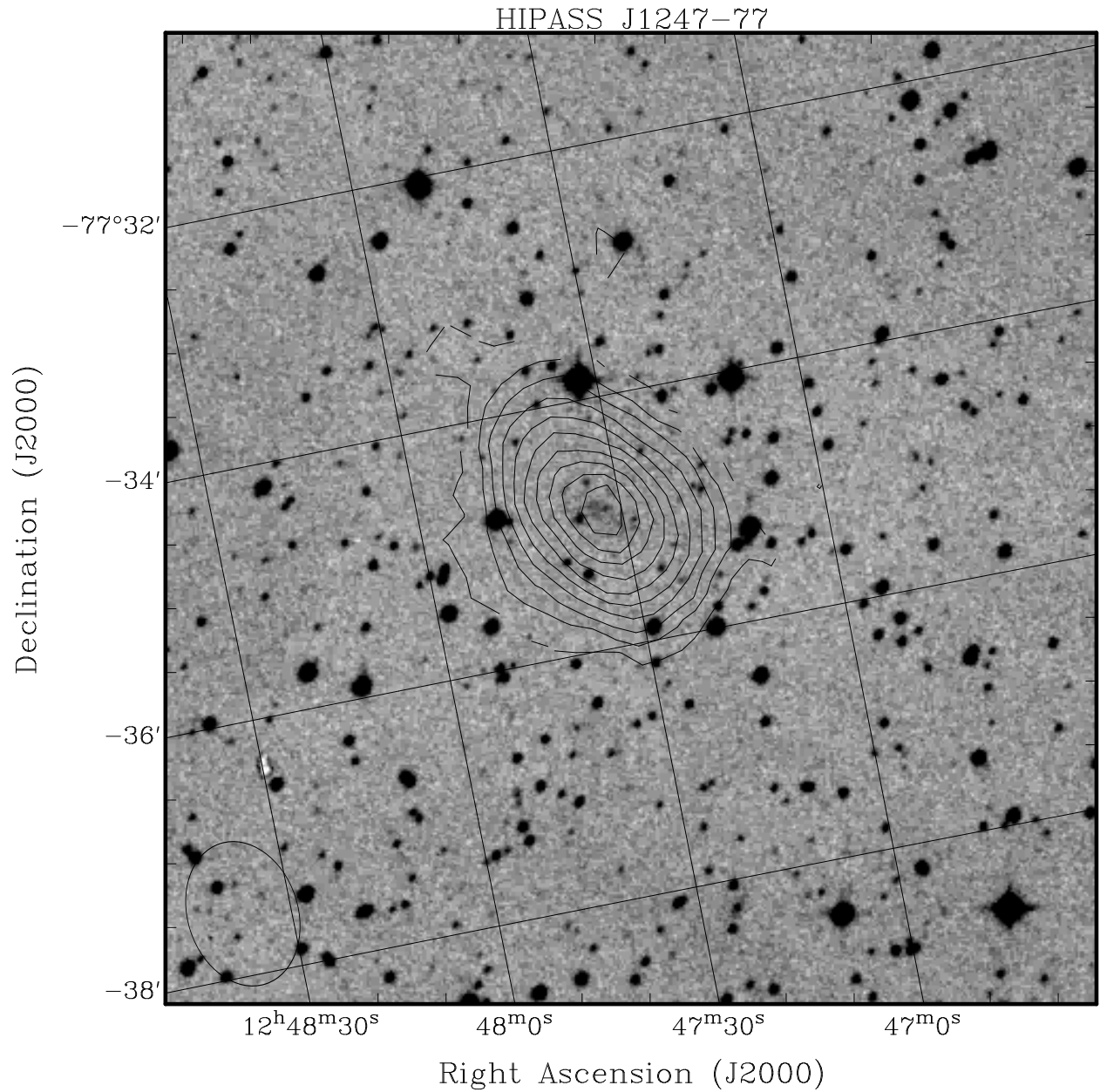


Fig. 15.— ATCA observation of a previously uncatalogued low surface brightness galaxy, HIPASS J1247-77. This galaxy lies at a velocity of  $411 \text{ km s}^{-1}$ , and has an H I mass of just  $4.6 \times 10^6 M_{\odot}$  at the distance of 2.2 Mpc. The beam is shown in the bottom left corner of the image.



Table 1. South Celestial Cap HI Catalogue. Detections confirmed with Parkes narrow-band observations are marked with an asterisk, and HI detections with a confused optical counterpart are marked with a double dagger. [The complete version of this table is in the electronic edition of the Journal. The printed edition contains only a sample]

HIPASS Name	R.A. J2000	Dec. J2000	Vel km s <sup>-1</sup>	$\Delta V_{20}$ km s <sup>-1</sup>	$\Delta V_{50}$ km s <sup>-1</sup>	$S_{peak}$ Jy	$S_{int}$ Jy·km s <sup>-1</sup>	$\log M_{HI}$ $M_{\odot}$	Optical ID	$V_{opt}$ km s <sup>-1</sup>	Morphology
HIPASSJ0002-80	00:02:54.1	-80:20:21.1	1959	130	97	0.218	20.53	9.43	ESO 012- G 014	1953	SBm
HIPASSJ0014-70	00:14:01.2	-70:02:32.9	4190	105	78	0.120	8.15	9.76	ESO 050- G 006	4135	SBcd
HIPASSJ0019-77	00:19:50.6	-77:06:12.7	1790	140	118	0.171	16.78	9.26	ESO-LV 0280141	...	SBb <sup>‡</sup>
HIPASSJ0020-63	00:20:59.2	-63:52:35.9	1760	189	168	0.084	10.68	9.07	ESO 078- G 022	1775	Sb
HIPASSJ0032-64	00:32:02.2	-64:18:52.5	2661	465	390	0.113	32.22	9.94	AM 0029-643	...	Sb <sup>‡</sup>
HIPASSJ0039-76	00:39:39.6	-76:19:13.2	1758	99	69	0.053	3.49	8.56	...	...	dS0
HIPASSJ0040-63	00:40:54.0	-63:27:05.1	1713	194	157	0.174	24.92	9.41	ESO 079- G 005	1721	SBcd
HIPASSJ0046-80	00:46:03.4	-80:46:43.9	4109	523	267	0.082	21.14	10.14	ESO 013-IG 001	4169	Sa
HIPASSJ0049-66	00:49:57.4	-66:32:44.4	1666	142	113	0.057	5.33	8.71	ESO 079- G 007	1674	Sa*
HIPASSJ0050-75	00:50:33.8	-75:19:40.5	4363	350	233	0.045	8.31	9.80	...	...	dI*
HIPASSJ0100-68	01:00:01.2	-68:09:14.5	6994	405	180	0.055	10.90	10.35	ESO 051- G 011	6944	Sab
HIPASSJ0100-85	01:00:20.0	-85:32:31.5	4659	312	273	0.039	8.18	9.84	ESO 002- G 012	4640	Sc
HIPASSJ0102-65	01:02:48.3	-65:37:44.8	2311	425	358	0.082	21.97	9.64	NGC 0360	2284	Scd
HIPASSJ0102-80	01:02:48.1	-80:13:58.4	1812	173	151	0.085	10.77	9.07	ESO 013- G 009	1808	SBcd
HIPASSJ0107-69	01:07:27.0	-69:52:16.7	1506	266	242	0.197	39.64	9.47	NGC 0406	1509	SBc

Table 2: Derived parameters for the 27 galaxies detected with the ATCA

HIPASS Name	R.A. J2000	Dec. J2000	Vel km s <sup>-1</sup>	$\Delta V_{20}$ km s <sup>-1</sup>	$\Delta V_{50}$ km s <sup>-1</sup>	$S_{peak}$ Jy	$S_{int}$ Jy.km s <sup>-1</sup>	Obs	Array
HIPASSJ0039–76	00:39:08	–76:20:12	1739	92	56	0.076	3.1	Jun99	750
HIPASSJ0116–63	01:16:48	–63:30:01	2301	136	119	0.017	1.3	Jun99	750
HIPASSJ0159–83	02:00:11	–83:59:16	3498	109	93	0.045	3.0	Dec98	750
HIPASSJ0209–75	02:09:01	–75:56:11	1653	188	175	0.048	5.14	Oct97	375
HIPASSJ0305–69	03:05:24	–68:56:31	1364	131	117	0.033	2.4	May00	750
HIPASSJ0411–70	04:11:38	–70:14:13	7155	79	65	0.030	1.1	May00	750
HIPASSJ0511–72	05:11:34	–72:18:21	1525	92	72	0.064	3.8	Oct97	375
HIPASSJ0554–71	05:54:42	–71:55:50	1473	64	58	0.044	2.2	Oct97	375
HIPASSJ0729–75	07:28:43	–75:03:21	1118	136	80	0.092	6.3	Jun99	750
HIPASSJ0751–62	07:51:33	–62:19:59	6106	77	56	0.024	1.3	Dec99	375/750
HIPASSJ0908–64	09:08:21	–64:42:10	1839	73	39	0.073	3.4	Jun99	750
HIPASSJ1004–73	10:05:03	–73:51:15	1243	58	42	0.152	5.7	Jun98	750
HIPASSJ1150–69	11:51:35	–69:48:26	6810	73	26	0.035	1.2	May00	750
HIPASSJ1242–77	12:42:06	–77:55:19	2654	76	64	0.057	2.9	Jun98	750
HIPASSJ1247–77	12:47:35	–77:34:53	413	50	29	0.122	4.1	Jun98	750
HIPASSJ1339–72	13:39:23	–72:54:54	3220	149	136	0.032	2.4	Jun98	750
HIPASSJ1407–75	14:07:28	–75:53:24	2795	145	108	0.089	8.0	Jun98	750
HIPASSJ1456–72	14:56:42	–72:33:10	3110	154	121	0.041	3.2	May00	750
HIPASSJ1512–72	15:11:56	–72:51:28	3000	424	408	0.211	61.1	May00	750
HIPASSJ1648–69	16:48:13	–69:08:14	4683	352	313	0.105	16.1	Jun99	750
HIPASSJ1650–62	16:49:49	–62:33:05	4226	122	89	0.042	2.7	May00	750
HIPASSJ1705–68	17:05:55	–68:57:33	7826	348	288	0.021	3.5	Dec99	750
HIPASSJ1816–67	18:15:45	–67:01:36	3312	190	183	0.058	7.0	Jun99	750
HIPASSJ2039–63	20:39:01	–63:46:15	1644	65	52	0.091	4.1	Dec99	750
HIPASSJ2214–67	22:13:46	–67:24:19	3178	56	41	0.036	1.2	Jun99	750
HIPASSJ2247–73	22:48:14	–73:48:49	3378	167	154	0.013	1.3	Oct97	375
HIPASSJ2309–74	23:08:40	–74:49:52	2073	147	98	0.019	1.4	Jun98	750

Table 3: Characteristics of the SCC sample

Area surveyed	2400 deg <sup>2</sup>
Velocities surveyed	–1200 – 12,700 km s <sup>–1</sup>
Velocities catalogued	300 – 10610 km s <sup>–1</sup>
Average RMS	13 mJy beam <sup>–1</sup>
Number of Galaxies in Catalogue	536
New Galaxies	114
New redshifts (of catalogued galaxies)	134
Mass range	$5 \times 10^6 - 9 \times 10^{10} M_{\odot}$
Mean Velocity	3313 km s <sup>–1</sup>
Mean $\Delta V_{20}$	240 km s <sup>–1</sup>
Mean $\Delta V_{50}$	186 km s <sup>–1</sup>
Mean $M_{\text{HI}}/L_B$	1.7 $M_{\odot}/L_{\odot}$

Table 4: Characteristics of galaxies of different optical classification.

	Early Type	Early Spiral	Late Spiral	Late Type
$\langle M_{\text{HI}}/L_B \rangle$	1.8	2.0	2.2	3.2
Median $M_{\text{HI}}/L_B$	1.3	1.3	1.6	2.1
Number with measured $L_B$	8	63	118	54